

Data-Driven Optimization for Police Zone Design

Shixiang Zhu, He Wang, and Yao Xie

H. Milton Stewart School of Industrial and Systems Engineering, Georgia Institute of Technology, Atlanta, Georgia 30332, USA

Abstract

We present a data-driven optimization framework for redesigning police patrol zones in an urban environment. The objectives are to rebalance police workload among geographical areas and to reduce response time to emergency calls. We develop a stochastic model for police emergency response by integrating multiple data sources, including police incidents reports, demographic surveys, and traffic data. Using this stochastic model, we optimize zone redesign plans using mixed-integer linear programming. Our proposed design was implemented by the Atlanta Police Department in March 2019. By analyzing data before and after the zone redesign, we show that the new design has reduced the response time to high priority 911 calls by 5.8% and the imbalance of police workload among different zones by 43%.

Keywords— police operations, data analytics, queueing model, optimization

1 Introduction

In large urban areas, police departments often organize their patrol forces by dividing the geographical region of a city into multiple patrol *zones* (also known as *precincts*), and each zone is further divided into multiple *beats* (or *sectors*) (Larson 1972). The design of patrol zones affects the demand and capacity for police services in each beat/zone, as well as the travel time of patrol units—together, these factors will determine the police’s response time to emergency calls and crime events. Therefore, a good design of patrol zones is important for achieving efficient police operations.

In this paper, we propose a data-driven framework for redesigning police zones. The work is developed based on our collaboration with the Atlanta Police Department (APD) to redesign police zones in Atlanta, Georgia in a project that lasted from 2017 to early 2019. The APD is the main police force in the Metro Atlanta area, which is the ninth largest metropolitan area in the United States and home to 6 million people. The APD divides the geographical area of Atlanta into six *zones* and 81 beats (see Figure 1). One police patrol unit is usually assigned to each beat to patrol that area and respond to 911 calls. If the response unit is busy handling another incident, available patrol units in other beats of the same zone will be dispatched to answer calls originating from that beat. Patrol units in the same zone back up for each other, but they typically do not travel across

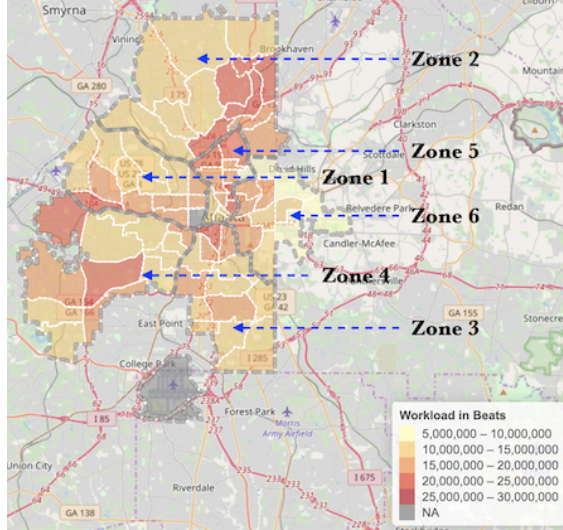


Figure 1: Atlanta police zone and beat design (prior to the redesign in March 2019). *Note:* Gray dashed lines represent the boundaries of the six zones. White lines represent the boundaries of the beats. The color in each beat indicates the average police workload level in 2017 (in seconds).

the zone boundaries unless there is a major incident. Under this dispatching policy, the system can be modeled as a spatially distributed queueing network (Larson 1974a, Larson and Odoni 1981).

The last zone and beat configuration in Atlanta (Figure 1) was designed in 2011. Since then, Atlanta has experienced significant population growth and urban development. The U.S. Census Bureau estimated that the population of Atlanta has increased by 15.8% from 2010 to 2017 (United States Census Bureau 2018). The population growth led to an increase in police workload, which was exacerbated by the difficulty faced by the APD in officer recruitment and retention. In 2018, the average response time to the highest priority 911 calls (e.g., violent crimes) in Atlanta was 9.5 minutes, which was above the national average (Fritz 2018). Moreover, changing demographics and traffic patterns in Atlanta created uneven police workloads among different regions. The colors in Figure 1 indicate the average workload in each beat, which we compiled from the 911 police incident report data in 2017. Higher workload in a beat often led to longer 911 call response time. For example, Zone 2, which is located in North Atlanta, had a higher than average workload due to its recent commercial development. From the police report data, we found that the average response time for the highest priority calls (e.g., carjacks or burglaries) was 13.5 minutes in Zone 2, whereas the average response time citywide for high-priority calls was 9.5 minutes. During the same period, Zone 2, a historically low-crime area, has experienced a rising number of car thefts, burglaries, and armed robberies (Habersham and Deere 2019).

The challenges faced by the Atlanta Police Department motivate us to develop a rigorous quantitative method using operations research for redesigning police zones. The method we proposed can be applied to other urban regions facing similar problems.

1.1 Paper Outline and Contributions

The contribution of our study is two-fold. First, we propose a general analytical framework for redesigning police patrol zones. This framework integrates statistical prediction for emergency call

arrivals and police service rates, stochastic modeling of police dispatching process, and optimization for zone redesign. Second, we describe our implementation process to the recent redesign in Atlanta and analyze the result after the implementation. The two components of our contribution are described below.

Our proposed framework integrates data analysis, statistical prediction, stochastic modeling, and optimization in an end-to-end design process. A summary of this framework is illustrated in Figure 2. Our objective of the zone design problem is to rebalance police workload, while guaranteeing short response time to 911 calls, by dividing a geographical area into several police zones. Our work complements the existing literature on *predictive policing* (Perry et al. 2013), which focuses primarily on statistical analysis and prediction, rather than prescription. Our work also contributes to the urban police operations literature by developing a comprehensive quantitative framework for zone redesign and analyzing the result of its implementation.

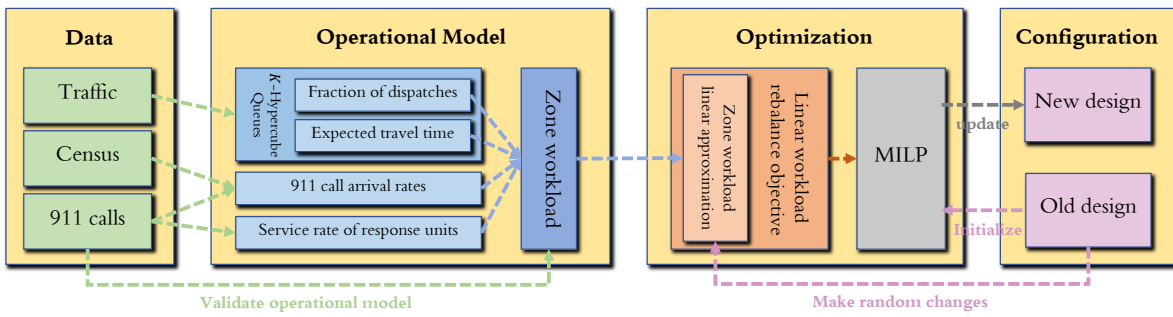


Figure 2: An illustration for the data-driven optimization framework of police zone redesign.

The basis of our design process is the modeling and predicting of 911 call events and police’s response and processing time. This is a challenging task because the occurrence of 911 call incidents is highly uncertain. To this end, we develop a spatial-temporal statistical model to predict the arrival rates of 911 calls and use a queueing model to capture the dynamics of patrol units’ response and movement. By integrating the statistical model and the queueing model, we obtain an prediction of police workloads. The workload prediction is further simplified by a parametric approximation, which is achieved using numerical simulations. The details of these procedures are presented in Section 3 and Section 4.

Section 5 discusses how to optimize zone designs. We show that the zone design problem can be formulated as a mixed-integer linear program (MILP). The objective function of the MILP measures workload imbalance across all zones, and the constraints of the MILP require zones to be contiguous and compact. Once the MILP solution is obtained, we use a local search heuristic to refine the solution in order to incorporate various design requirements specified by the APD.

In Section 6, we present the implementation results. To minimize the impact of zone change, the final redesign plan we proposed to the APD suggests changing four out of 81 beats. After presenting the design and numerical findings to the APD and the Atlanta City Council, our plan was implemented in March 2019 (Atlanta Police Department 2019). We analyze the police report data from March 2019 and March 2020 and show that the zone redesign has resulted in a reduction of police workload imbalance and a decrease in police response time and travel time for 911 calls.

2 Literature Review

The study of police zone design and police patrol operations has an extensive history dating back to the 1960s. The books by [Larson \(1972\)](#), [Ríos-Mercado \(2020\)](#) and the survey papers by [Chaiken and Larson \(1972\)](#), [Green and Kolesar \(2004\)](#) provide a comprehensive summary of this field. Below, we review the related literature from three aspects: crime prediction, stochastic modelling of police operations, and optimization for police patrol zones.

Prediction. Big data and analytics techniques have gained popularity in policing over the last two decades. Several large police departments in the U.S. have been experimenting with predictive policing that uses historical crime data to predict future crime activities ([Perry et al. 2013](#)). For example, [Levine et al. \(2017\)](#) reported how a predictive policing system was implemented by the New York City Police Department. However, a downside of predictive policing is that it does not prescribe how predictive crime forecasts should be translated into police's operational decisions. [Saunders et al. \(2016\)](#) analyzed the predictive policing program of the Chicago Police Department using a quasi-experiment and found that the effect of predictive policing was not statistically significant. The practice of predictive policing has also drawn criticisms from civil rights groups for proliferating racial profiling ([Edwards 2016](#)).

Stochastic Modeling. Police emergency response systems can be viewed as queueing systems where servers and customers are spatially distributed, and servers must travel to customer locations. [Larson \(1974a\)](#) propose a hypercube queueing model for urban emergency services. This hypercube queue model is also studied in [Chelst and Jarvis \(1979\)](#), [Larson and Odoni \(1981\)](#). [Bammi \(1975\)](#) considers a beat allocation model where the beat design is fixed, but the patrol units can be moved or shared among different beats.

Optimization. [Gass \(1968\)](#) is one of the earliest works that study optimal police beat allocation using integer programming. [Mitchell \(1972\)](#) studies an optimal beat selection problem. [Bodily \(1978\)](#) considers fairness issues of police zone design. [Benveniste \(1985\)](#) proposes a stochastic optimization model that combines zoning and facility location. More recently, [Curtin et al. \(2005, 2010\)](#) propose maximal covering models for police patrol area design. [Cheung et al. \(2015\)](#), [Chow et al. \(2015\)](#) consider facility location models for police operations. [Bucarey et al. \(2015\)](#) formulates the police districting problem as an enriched p -median model. [Camacho-Collados et al. \(2015\)](#), [Liberatore and Camacho-Collados \(2016\)](#) introduce a multi-criteria police districting problem that provides a balance between efficiency and workload homogeneity. [Piyadasun et al. \(2017\)](#) redesign police patrol beats by clustering methods. [Chen et al. \(2019\)](#) proposes a street-level design for urban police districting. Implementation of police zone redesign has been reported for Boston, MA ([Larson 1974b](#)), Buffalo, NY ([Sarac et al. 1999](#)), and Tucson, AZ ([Kistler 2009](#)).

Unlike most of the existing literature that focuses on one of the three aspects above, our paper presents a comprehensive framework that integrates prediction, stochastic modelling, and optimization for the police zone design problem. We apply this framework to police zone redesign in Atlanta and evaluate the effect of the redesign.

Aside from the police zone design problem, other types of geographical districting problems have also been studied in the operations research literature, including *political districting* ([Hess et al. 1965](#), [Garfinkel and Nemhauser 1970](#)) and *school districting* ([Ferland and Guénette 1990](#)). Several papers ([Weaver and Hess. 1963](#), [Mills 1967](#), [Morrill 1973, 1976](#), [Vickrey 1961](#), [D'Amico et al. 2002](#)) apply meta-heuristics for geographical districting. These studies consider design criteria such as contiguity ([Grofman 1985](#), [Mills 1967](#), [Garfinkel and Nemhauser 1970](#), [Nagel 1972](#), [Mehrotra et al. 1998](#), [Vickrey 1961](#)) and compactness ([Garfinkel and Nemhauser 1970](#), [Niemi 1990](#), [Yong 1988](#)). In this paper, we use a network flow based formulation by [Shirabe \(2009\)](#) to impose contiguity constraints. However, the political districting problem and the school districting

problem have different objectives than police districting. Political districting and school districting are often formulated as deterministic optimization problems, but police districting must take into under uncertainty associated with crime occurrence and police service time. Specifically, our model considers the queueing aspect of police patrol systems which have multiple moving servers (i.e., patrol units). The workload for each server is stochastic, and the servers' status depends on each other. In addition, changes to the zone configuration will impact the operational dynamics of the zone, including the travel time of servers, and the number of 911 calls needs to be served. These factors are included in our workload prediction model and optimization model.

3 Police Patrol and Emergency Response Model

In this section, we present a stochastic model for the police patrol and emergency responses. We begin with a description of police patrol practices, which will aid our discussion later. We then model the patrol units as a queueing system in Section 3.2. In Section 3.3, we derive expressions for several performance measures. The notations defined in this section are summarized in Table 1.

Table 1: Summary of Notations

Section	Notation	Description
3.2.1	$\mathcal{I} = \{i = 1, \dots, I\}$	Set of all beats
	$\mathcal{K} = \{k = 1, \dots, K\}$	Set of all zones
	$D = (d_{ik})_{i \in \mathcal{I}, k \in \mathcal{K}}$	Districting design matrix indicating if beat i is assigned to zone k , $i \in \mathcal{I}$, $k \in \mathcal{K}$
	$\mathcal{I}^{(k)}$	Set of beats assigned to zone $k \in \mathcal{K}$
	$N^{(k)}$	Total number of beats assigned to zone $k \in \mathcal{K}$
	λ_i	911 calls-for-service arrival rate in beat $i \in \mathcal{I}$
3.2.2	μ	Service rate of each response unit
	$B^{(k)}, S^{(k)}$	The unsaturated and saturated states for zone $k \in \mathcal{K}$
	$H^{(k)} = (\eta_{nj}^{(k)})$	Optimal unit dispatched to beat $j \in \mathcal{I}^{(k)}$ under unsaturated states $B_n^{(k)}$
	$Q^{(k)} = (q_{nm}^{(k)})$	Transition rate matrix associated with unsaturated states
3.3	$T = (\tau_{ij})$	Average travel time from beat i to beat j , $\forall i, j \in \mathcal{I}$
	$E_{ij}^{(k)}$	Set of states in which unit $i \in \mathcal{I}^{(k)}$ is an optimal unit to assign to a call from beat $j \in \mathcal{I}^{(k)}$
	$\rho_{ij}^{(k)}$	Fraction of all calls that send unit $i \in \mathcal{I}^{(k)}$ to beat $j \in \mathcal{I}^{(k)}$ in zone k
	$\xi_i^{(k)}$	Expected travel time of unit $i \in \mathcal{I}^{(k)}$
	$w^{(k)}(D)$	Total workload of zone $k \in \mathcal{K}$ given districting D

3.1 Background

Police departments usually divide the geographical areas of a city into several *zones*, and each zone is comprised of several *beats*. For example, Atlanta is currently divided into 6 zones and 81 beats (Atlanta Police Department 2020). New York City, which has the largest police department in the U.S., contains 77 precincts (equivalent to zones) and 302 sectors (equivalent to beats) (New York City Government 2020). Many cities, including Atlanta and New York City, have fixed patrol districts, although in some other cities the districting may be changed during a 24-hour period if there are significant changes in the pattern of calls throughout the day. We assume the zone districting is fixed over time in this paper.

Typically, one police patrol unit (e.g., a patrol car) is assigned to each beat, where the unit has primary responsibility. When a patrol unit is not busy serving any active calls, it traverses its home beat to perform preventive patrol. If a call of service is received, the dispatcher will try to send an available unit in the zone to the location of the reported incident. As a result, a patrol unit

may be dispatched to any location within its zone, possibly *outside* its home beat. If unfortunately, all units in that zone are busy, the call must wait in a queue until a patrol unit becomes available later. We treat each zone as an independent system — in practice, there are very few dispatches across zone boundaries, due to both long travel time and administrative difficulty (Larson 1972).

We can thus describe the timeline of a reported incident as follows (see an illustration in Figure 3): When a 911 call arrives, the dispatcher will try to assign an available patrol unit in the zone of that incident to process it. If all patrol units are busy, the request needs to wait in a queue until at least one unit in that zone becomes available. We refer to the duration between the call arrival time and the dispatch time as the *waiting time*. Once dispatched, the patrol unit travels from its current location to the location of the reported incident. The *response time* is thus the sum of waiting time in the queue and the travel time. After arriving at the scene, we refer to the amount of time spent on processing the incident as the *on-scene time*. The *service time* for the patrol units to process that incident is equal to the sum of the *travel time* and the *on-scene time*.

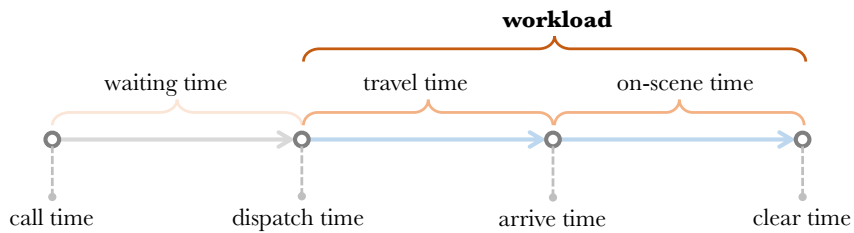


Figure 3: The timeline to process a police incident.

In line with practice, we make the following assumptions on the dispatching rule: (1) The number of patrol units allocated to each zone is equal to the number of beats; for simplicity, we do not consider backup units. (2) In response to each call for police service, the nearest available patrol unit is dispatched to the scene of the request; a major incident may require multiple police units to respond, but we ignore such possibility since these incidents are rare. (3) If no unit is available in the zone of the request, the call enters a queue with other backlogged calls, which is processed according to the first-come-first-served (FIFO) rule. (4) Upon completion of the service, a patrol unit is either dispatched to a call waiting in the queue, or it immediately returns to its home beat if the queue is empty. In the formulation of the stochastic model below, we assume returning to the home beat is instantaneous.

3.2 Model Formulation

3.2.1 Zone Districting

Consider the police districting problem with K zones and I beats ($K < I$). Let $k \in \mathcal{K} = \{1, \dots, K\}$ denote the set of zones. Let $i \in \mathcal{I} = \{1, \dots, I\}$ denote both the set of beats, as well as the set of police patrol units which are assigned to these beats. We assume that the shape of each beat is given. A particular zone districting design is thus a graph partition of I beats into K zones. Let the binary decision variable $d_{ik} \in \{0, 1\}$ denote whether beat i is assigned to zone k . The districting decision is represented by a matrix $D = (d_{ik}) \in \{0, 1\}^{I \times K}$. For each $i \in \mathcal{I}$, we have $\sum_{k=1}^K d_{ik} = 1$. Given a zone design D , the set of beats assigned to zone k is denoted by $\mathcal{I}^{(k)} = \{i \mid d_{ik} = 1\} \subseteq \mathcal{I}$ and the number of beats in zone k is denoted by $N^{(k)} = \sum_{i \in \mathcal{I}} d_{ik}$. Throughout this section, we assume the zone districting matrix D is fixed. In Section 5, we will consider optimization over the zone districting.

3.2.2 Hypercube Queue Model

For a fixed zone configuration, the dynamics of patrol units in each zone is independent, since we assume patrol units do not respond to requests from a different zone than they are assigned (see Section 3.1). Within each zone, the movement and workload of patrol units are quite complex, as they are determined by the zone districting, the dispatch rule, and the beat-to-beat travel time. We model the dynamics based on the *hypercube queue model* proposed by Larson (1974a).

For a given zone $k \in \mathcal{K}$, recall that the set of patrol units in this zone is denoted by $\mathcal{J}^{(k)}$. Let $N^{(k)} = |\mathcal{J}^{(k)}|$ be the total number of patrol units, which is equal to the number of beats in zone k . We assume that the arrivals of 911 calls in beat $i \in \mathcal{J}$ follow a time-homogeneous Poisson process with rate λ_i . Let $\lambda^{(k)} = \sum_{i \in \mathcal{J}^{(k)}} \lambda_i$ be the aggregate call arrival rate in zone k . Denote the average travel time between two arbitrary beats as a matrix $T = (\tau_{ij}) \in \mathbb{R}_+^{I \times I}$, where τ_{ij} is the average travel time from beat i to beat j . The service time of each patrol unit is i.i.d. and follows an exponential distribution with mean $1/\mu$ ¹. We require $\lambda^{(k)} < \mu N^{(k)}$ for the stability of this queueing system.

The system state depends on the status of all the units in this zone, and the number of calls in queue to be processed. Based on whether there is any available unit, the state space (denoted by $C^{(k)}$) can be divided into two parts: (1) *unsaturated states*: the states where the queue for unprocessed calls is empty. These states can be represented by a hypercube in dimension $N^{(k)}$ (hence the name “hypercube queue model”). An example with $N^{(k)} = 3$ is shown in Figure 4. Each vertex of the hypercube corresponds to a state $B^{(k)} = (b_i)_{i \in \mathcal{J}^{(k)}}$, where unit i is busy processing a call if $b_i = 1$ and idle if $b_i = 0$. Considering the state $B^{(k)}$ as a vector of binary numbers, we index the state by its corresponding decimal form $B_n^{(k)}$ where $n = \sum_{j=1}^{N^{(k)}} 2^{j-1} b_j$. (2) *saturated states*: the states where the queue for unprocessed calls is non-empty. By definition, all patrol units are busy under saturated states. We denote these states by $\{S_n^{(k)}\}_{n \geq 1}$; the state $S_n^{(k)}$ indicates that there are exactly n calls waiting in queue for zone k .

We now define the state transition rates. For the saturated states, the transition rate from $S_n^{(k)}$ to $S_{n+1}^{(k)}$, as well as from the transition rate from $B_{2^{N^{(k)}}-1}^{(k)}$ to $S_1^{(k)}$, is $\lambda^{(k)}$. The transition rate from $S_{n+1}^{(k)}$ to $S_n^{(k)}$, as well as the transition rate from $S_1^{(k)}$ to $B_{2^{N^{(k)}}-1}^{(k)}$, is $\mu N^{(k)}$.

For the unsaturated states, we define the transition rate matrix $Q^{(k)} = (q_{nm}^{(k)})$ for zone k , where $q_{nm}^{(k)}$ (for $n \neq m$) denotes the rate departing from the n -th unsaturated state and arriving in the m -th unsaturated state. Diagonal entries $q_{nn}^{(k)}$ are defined such that $q_{nn}^{(k)} = -\sum_{m:m \neq n} q_{nm}^{(k)}$ and therefore the rows of the matrix sum to zero.

There are two classes of transitions on the hypercube: *upward transitions* that change a unit’s status from idle to busy; *downward transitions* that do the reverse. Let d_{nm} denote the Hamming distance between two vertices B_n and B_m on the hypercube. We define the “upward” Hamming distance as $d_{nm}^+ = |B_n^C \cap B_m|$ and the “downward” Hamming distance as $d_{nm}^- = |B_n \cap B_m^C|$, where $|B|$ denote the number of binary “one” in B (i.e., the number of busy units), and B^C denote the complement of B . The downward transition rate from state B_n to the adjacent states B_m with $d_{nm}^- = 1$ is always $q_{nm}^{(k)} = \mu$. The upward transition rates, however, will depend on the dispatch rule (denoted by $H^{(k)}$) when a call is received. As mentioned in Section 3.1, we assume that when

¹This means that service time is independent of travel time. This assumption is necessary to derive a tractable hypercube queue model. Otherwise, if the service time depends on the unit and beat locations, the hypercube queue model will have a much larger state space (Jarvis 1975). Larson and Odoni (1981) (Section 5.4.2) argues that this assumption is often a good approximation in practice since the variance in police service time is much larger than the variance in travel time.

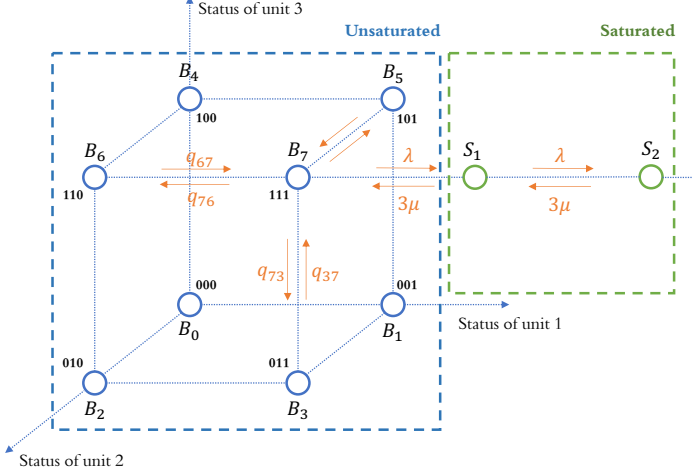


Figure 4: The state-space of a hypercube queue model with three beats. (For simplicity, we omit the superscript for zone index.)

a call is ready to be processed, the nearest available unit with the minimum mean travel time to the location of the call is dispatched. That is, if the call is in beat i and the system state is $B_n^{(k)}$, the index of the unit dispatched is $\eta_{ni}^{(k)} := \arg \min_{j: b_j=0, b_j \in B_n^{(k)}} \tau_{ji}$ (we assume there are no ties in the mean travel time matrix). The upward transition rate from state B_n to an adjacent states B_m with $d_{nm}^+ = 1$, can be obtained by $q_{nm} = \sum_{i: \eta_{ni}^{(k)} = j, \forall i} \lambda_i$, where j is the index of the unit dispatched and satisfies $m = n + 2^{j-1}$. To illustrate how this dispatch rule works, we give a detailed example in Figure 5.

The steady-state probabilities of this system are determined from the balance equations. Let $\mathbb{P}\{B_m^{(k)}\}$ and $\mathbb{P}\{S_n^{(k)}\}$ denote the probability that system is occupying state $B_m^{(k)}$ and $S_n^{(k)}$ under steady-state conditions. For unsaturated states, we have

$$\begin{aligned} \left(\lambda^{(k)} + \mu |B_m^{(k)}| \right) \mathbb{P}\{B_m^{(k)}\} &= \sum_{\{B_n^{(k)} : d_{nm}^+ = 1\}} q_{nm} \mathbb{P}\{B_n^{(k)}\} + \sum_{\{B_n^{(k)} : d_{nm}^- = 1\}} \mu \mathbb{P}\{B_n^{(k)}\}, \quad \forall m = 1, \dots, 2^{N^{(k)}} - 2, \\ \left(\lambda^{(k)} + \mu N^{(k)} \right) \mathbb{P}\{B_m^{(k)}\} &= \sum_{\{B_n^{(k)} : d_{nm}^+ = 1\}} q_{nm} \mathbb{P}\{B_n^{(k)}\} + \mu N^{(k)} \mathbb{P}\{S_1^{(k)}\}, \quad \text{for } m = 2^{N^{(k)}} - 1, \end{aligned} \quad (1)$$

where $\lambda^{(k)} = \sum_{i \in \mathcal{J}^{(k)}} \lambda_i$ is the aggregate call arrival rate in zone k . For saturated states, we have

$$\left(\lambda^{(k)} + \mu N^{(k)}\right) \mathbb{P}\{S_n^{(k)}\} = \lambda^{(k)} \mathbb{P}\{S_{n-1}^{(k)}\} + \mu N^{(k)} \mathbb{P}\{S_{n+1}^{(k)}\}, \quad \forall n \in \mathbb{Z}_+.$$

In addition, we require that the probability sum to one, namely

$$\sum_{m=0}^{2^{N(k)}-1} \mathbb{P}\{B_m^{(k)}\} + \sum_{n=1}^{\infty} \mathbb{P}\{S_n^{(k)}\} = 1.$$

We note that although the number of saturated states is infinite, it can be expressed in closed-form as in an $M/M/c$ queue. The main challenge for computing the steady-state distribution is that the number of *unsaturated* states on the hypercube grows exponentially with the number of beats. In Section 3.4, we propose an efficient computation method to approximate the steady-state distribution, which exploits the fact that the hypercube queue model has a sparse transition matrix.

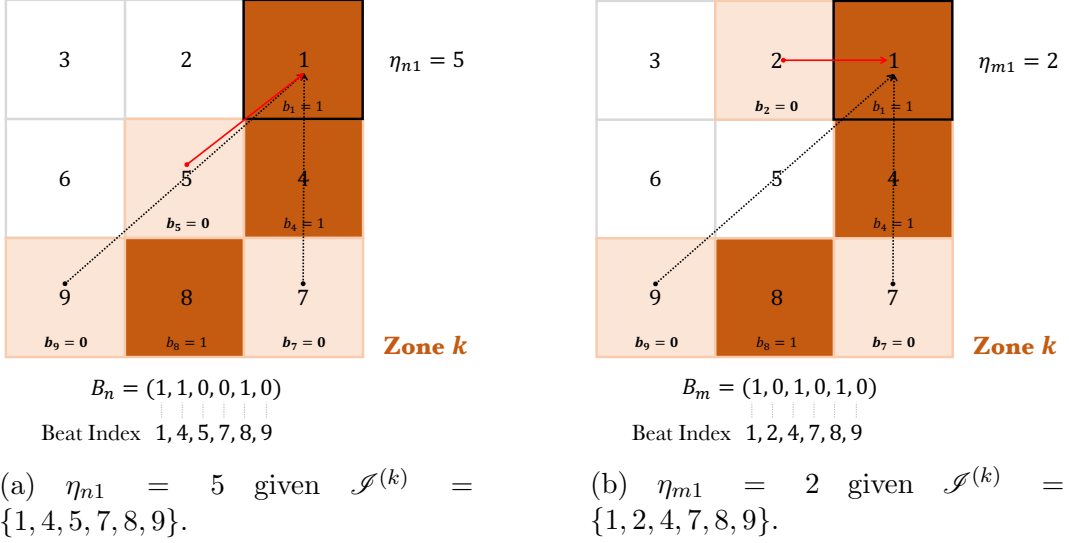


Figure 5: Two examples show how districting decision affects the dispatch rule. Each numbered block represents a beat. The colored area represents a zone comprised of six beats. The darker blocks represent the corresponding patrol unit i is busy ($b_i = 1$). Euclidean distance is used as a proxy for travel time between beats. The arrows indicate all possible dispatches, and the red line indicates the optimal dispatch with the shortest travel time.

3.3 Measures of Performance

Using the steady-state distribution of the hypercube queue model, we now derive several performance measures, which will guide our zone design decision in Section 5.

3.3.1 Fraction of Dispatches

To understand how often a patrol unit travels to different beats in the zone, it is critical to know how many calls in each beat have been assigned to a given unit. The fraction of dispatches in zone k that send unit $i \in \mathcal{I}^{(k)}$ to beat $j \in \mathcal{I}^{(k)}$, denoted by $\rho_{ij}^{(k)}$, can be divided into two terms: (1) $\rho_{ij}^{(k,1)}$ the fraction of dispatches that incurs no queue delay, and (2) $\rho_{ij}^{(k,2)}$ the fraction of dispatches that incurs a positive queue delay. The fraction of dispatches $\rho_{ij}^{(k)}$ can be expressed as

$$\rho_{ij}^{(k)} = \underbrace{\sum_{B_n^{(k)} \in E_{ij}^{(k)}} \frac{\lambda_j}{\lambda^{(k)}} \mathbb{P}\{B_n^{(k)}\}}_{\rho_{ij}^{(k,1)}} + \underbrace{\frac{\lambda_j P'_Q}{\lambda^{(k)} N^{(k)}}}_{\rho_{ij}^{(k,2)}}, \quad (2)$$

where $P'_Q = \sum_{m=1}^{\infty} \mathbb{P}\{S_m^{(k)}\} + \mathbb{P}\{B_{2^{N^{(k)}}-1}^{(k)}\}$ specifies the probability that a randomly arriving call incurs a queue delay; the set $E_{ij}^{(k)} = \{B_n^{(k)} \mid \eta_{nj}^{(k)} = i, n = 1, \dots, 2^{N^{(k)}} - 1\}$ contains all the unsaturated states in which unit i is the nearest available unit to assign to a call from beat j , which is determined by the dispatch rule $H^{(k)} = (\eta_{ni}^{(k)})$. Equation (2) can be found in Larson (1974a), so we omit the proof. Note that in Equation (2), the number of beats in zone k ($N^{(k)}$), the dispatch rule ($H^{(k)}$), and the steady-state probability ($\mathbb{P}\{B_n^{(k)}\}$, $\mathbb{P}\{S_m^{(k)}\}$) depends on the districting decision.

3.3.2 Expected Travel Time

Another key measure of performance is the travel time that a unit takes for a single dispatch. The travel time is affected by both the beat-to-beat travel time τ_{ij} and the fraction of dispatches $\rho_{ij}^{(k)}$. The beat-to-beat time $T = (\tau_{ij})$ can be estimated from the real traffic data, which will be discussed in Section 4. The fraction of dispatches critically depends on the utilization factor of the hypercube queue system. If the utilization is low, most calls can be processed by units close to their home beats, resulting in short travel time. However, if the system is congested, calls must wait in the queue, which will be processed in an FCFS basis. Each patrol unit is equally likely to process calls that incur a queue delay, regardless of their locations. This will lead to longer travel time.

To derive the equation for the expected travel time for zone $k \in \mathcal{K}$, we denote the expected travel time of unit i for a single dispatch as $\xi_i^{(k)}$, the expected travel time for a call in beat j as $T_j^{(k)}$, and the zone-wide mean travel time as $\bar{T}^{(k)}$. Using the result in Section 3.3.1, $\xi_i^{(k)}$ can be expressed as the weighted sum of mean travel times τ_{ij} for all beats j in zone k given the dispatch fraction $\rho_{ij}^{(k)}$. Specifically, the average travel time of unit i in zone k can be expressed (see Larson 1974a, Larson and Odoni 1981) as

$$\xi_i^{(k)} = \frac{\sum_{j \in \mathcal{J}^{(k)}} \rho_{ij}^{(k,1)} \tau_{ij} + \bar{T}_Q^{(k)} P'_Q / N^{(k)}}{\sum_{j \in \mathcal{J}^{(k)}} \rho_{ij}^{(k,1)} + P'_Q / N^{(k)}}, \quad (3)$$

where $\bar{T}_Q^{(k)} = \sum_{i \in \mathcal{J}^{(k)}} \sum_{j \in \mathcal{J}^{(k)}} \lambda_i \lambda_j \tau_{ij} / (\lambda^{(k)})^2$ is the mean travel time for calls that incur a positive queue delay and P'_Q is defined in Equation (2). Similarly, the expected travel time for calls in beat j is

$$T_j^{(k)} = \frac{\sum_{i=1}^{N^{(k)}} \rho_{ij}^{(k,1)} \tau_{ij}}{\sum_{i=1}^{N^{(k)}} \rho_{ij}^{(k,1)}} (1 - P'_Q) + \sum_{i=1}^{N^{(k)}} \frac{\lambda_i \tau_{ij}}{\lambda^{(k)}} P'_Q.$$

The zone-wide mean travel time is

$$\bar{T}^{(k)} = \sum_{i=1}^{N^{(k)}} \sum_{j \in \mathcal{J}^{(k)}} \rho_{ij}^{(k,1)} \tau_{ij} + P'_Q \bar{T}_Q^{(k)}.$$

3.3.3 Response Time.

The response time for a call includes both the travel time for the patrol unit to arrive at the scene and the waiting time if the call incurs a positive queue delay. Therefore, the average response time for calls in beat j is

$$T_j^{(k)} + \sum_{m=1}^{\infty} \frac{m+1}{\mu N^{(k)}} \mathbb{P}\{S_m^{(k)}\} + \frac{1}{\mu N^{(k)}} \mathbb{P}\{B_{2^{N^{(k)}}-1}^{(k)}\}.$$

As mentioned earlier, the infinite sum in the second term can be solved in closed form as in an M/M/c queue. The zone-wide mean response time is

$$\bar{T}^{(k)} + \sum_{m=1}^{\infty} \frac{m+1}{\mu N^{(k)}} \mathbb{P}\{S_m^{(k)}\} + \frac{1}{\mu N^{(k)}} \mathbb{P}\{B_{2^{N^{(k)}}-1}^{(k)}\}.$$

3.3.4 Patrol Unit Workload

Finally, we consider the workload of the patrol units in each zone. In Section 5, we will consider districting designs that balance the workload across zones, so this metric will play a vital role in defining the optimization objective. The workload of patrol unit i in zone k is

$$w_i^{(k)} = \sum_{n: (B_n^{(k)})_i = 1} \mathbb{P}\{B_n^{(k)}\} + \sum_{m=1}^{\infty} \mathbb{P}\{S_m^{(k)}\}.$$

Here, we introduce the districting decision D in defining the zone workload and it will be used in the objective function of our redistricting optimization in Section 5. The total workload for all patrol units in zone k is simply

$$w^{(k)}(D) = \sum_{i \in \mathcal{J}^{(k)}} w_i^{(k)}. \quad (4)$$

Note that the workload for zone k depends on the decision variable D through $\mathcal{J}^{(k)}$. A detailed explanation is given below.

3.3.5 Dependence of Performance Measures on the Districting Decision

A zone districting decision D divides the entire geographical region into K police zone, or K hypercube queue models. The dynamics between the above performance measures and the beat-to-zone allocations are quite complex, as the parameters of K hypercube queues are endogenously determined by the decision of beat allocation. As shown in Figure 6, the police zone workload $w^{(k)}(D)$ depends on decision D through a long dependence chain. Specifically, given a particular decision D , the beats will be divided into K zones, where zone $k \in \mathcal{K}$ corresponds to a set of beats $\mathcal{J}^{(k)}(D)$. This leads to a unique combination of K hypercube queues, where their state spaces $\{C^{(k)}\}_{k \in \mathcal{K}}$ and dispatch preferences $\{H^{(k)}\}_{k \in \mathcal{K}}$ are jointly controlled by how decision D partition the beats. By solving the linear equation system formed by the generator matrix $Q^{(k)}$ for each hypercube, we can obtain K steady-state distributions $\{\pi^{(k)}\}_{k \in \mathcal{K}}$. Accordingly, we can compute the performance measures $\xi_i^{(k)}(D), \rho_{ij}^{(k)}(D)$ for each hypercube queue based on their steady-state distribution. The unknown police zone workload $w^{(k)}(D)$ for K zones given a particular decision can be evaluated through the above process.

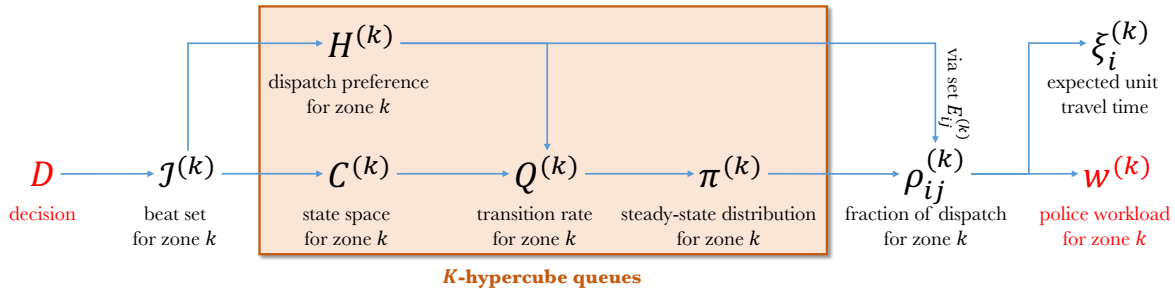


Figure 6: The dependence diagram for the key variables in the K -hypercube model.

3.4 Efficient Computation Method

Performing workload estimation efficiently is critical to search for the optimal zone design in the solution space. Take Atlanta as an example; there are more than 2,000 possible ways to shift the existing design even with less than only four changes that are allowed to make. Each zone in one particular design corresponds to a unique hypercube queue, where its zone workload needs to be re-evaluated separately.

A critical step for obtaining police zone workload estimation given a decision is to compute the steady-state distribution.

Let $\lambda^{(k)} = \sum_{i \in \mathcal{J}^{(k)}} \lambda_i$ be the total call arrival rate in zone k . It is clear that for zone k , if the system is in some state $B_n^{(k)}$ with $|B_n^{(k)}|$ servers busy, the total transition rate “downward” to states with one less busy server is $|B_n^{(k)}| \mu$ and the total transition rate “upward” to states with one more busy server is λ (except for $|B_n^{(k)}| = N^{(k)}$, in which case the upward transition rate is zero). Thus, if we aggregate states according to the numbers of servers busy, we obtain the well-known M/M/c multi-server queuing system. Then the steady-state probabilities in the saturated state set $\{S_n^{(k)}\}_{n \geq 1}$ is given by closed-form expression:

$$\mathbb{P}\{S_n^{(k)}\} = \frac{\frac{(\lambda^{(k)}/\mu)^{N^{(k)}}}{N^{(k)}!} \left(\frac{\lambda^{(k)}}{\mu N^{(k)}}\right)^n}{\sum_{s=0}^{N^{(k)}-1} \frac{(\lambda^{(k)}/\mu)^s}{s!} + \frac{(\lambda^{(k)}/\mu)^{N^{(k)}}}{N^{(k)}!} \frac{1}{1-\lambda^{(k)}/(\mu N^{(k)})}}, \quad \text{for all } n \in \mathbb{Z}_+.$$

Let the row vector $\pi^{(k)} = (\mathbb{P}\{B_m^{(k)}\})$ denote the steady-state probabilities in the unsaturated state set $C^{(k)}$. Then the balance equations (1) can be written compactly as

$$\pi^{(k)} = \pi^{(k)}(I^{(k)} + Q^{(k)}/\gamma^{(k)}),$$

where $I^{(k)}$ is the identity matrix (of the same size as $Q^{(k)}$) and $\gamma^{(k)} = \max |q_{ii}^{(k)}|$ is the largest absolute value on the diagonal of $Q^{(k)}$. The matrix $(I^{(k)} + Q^{(k)}/\gamma^{(k)})$ is the probability transition matrix of a discrete-time Markov chain obtained through uniformization of the original continuous-time Markov chain.

Theoretically, the solution to this set of equations requires a matrix inversion. However, the size of the matrix is equal to $2^{2N^{(k)}}$, thus becoming huge for even moderate values of $N^{(k)}$. Fortunately, due to the sparsity of the transition rate matrix, we can find the stationary distribution $\pi^{(k)}$ iteratively by the power method. More specifically, given the transition rate matrix $Q^{(k)}$ and an initial vector $\pi_0^{(k)}$, compute $\pi_t^{(k)} = \pi_{t-1}^{(k)}(I^{(k)} + Q^{(k)}/\gamma^{(k)})$ for $t = 1, 2, \dots$, until the distance (e.g. the sup norm) between $\pi_t^{(k)}$ and $\pi_{t-1}^{(k)}$ is small enough.

4 Model Estimation and Workload Prediction

In this section, we present an approach to estimate the hypercube queue model parameters presented in the last section using real data provided by the Atlanta Police Department (APD) and other sources. We first introduce in Section 4.1 the three data sets that we used for estimation. Then we describe our call arrival rate and workload prediction method in Section 4.2. We validate the performance of our estimated model in Section 4.3.

4.1 Data Sets

We have utilized three key data sets for police workload prediction:

1. *911 Call Data*: the APD provides electronic records of police reports, where each record consists of detailed information about a 911 call, including call time, dispatch time, arrive time, clear time, and location. Using this data set, we can estimate the 911 call arrival rates for each beat in past years and the service rate of response units.
2. *Dispatch Travel Data*: the APD also provided travel information of each dispatch, including the departure time, location, and the arrival time, location. We estimate the beat-to-beat time by averaging the time response units traveling from one beat to another beat.
3. *American Community Survey*: the U.S. Census Bureau provides the American Community Survey (ACS), which includes comprehensive information about the population, demographic, and economic status of different areas of Atlanta. Some demographic factors are particularly useful for us in making a prediction of future workload (by correlating city's socio-economic profile with the workload), and these factors contain essential information about the development and economic growth of the city. Here, we choose population, number of housing unit, school enrollment, median household income, median number of rooms, media age, median house price, and average year built from the ACS as explanatory variables in our predictive model. Unlike the Census, which takes place every ten years, the ACS is conducted once a year.

4.2 Workload Estimation

We obtained the three data sets described above for five years from 2013 to 2017. This enabled us to fit the hypercube queue model described in Section 3 to predict the future workload.

4.2.1 Call Arrival Rate Prediction

Predicting the call arrival rate is particularly challenging. Although the model in Section 3 assumes the call arrival rates are time-homogeneous, we observe in the actual data that the call arrival rates have a significant seasonality pattern and yearly trend (show in Figure 9 (b)), as well as correlation over adjacent geographical areas. Therefore, we propose a spatio-temporal model to predict future call arrival rates.

We index the five years from 2013 to 2017 by $\ell \in \mathcal{L} = \{1, \dots, L\}$, $L = 5$. Let $\lambda_{i\ell} \in \mathbb{R}_+$ represent 911 call arrival rates of beat i in year ℓ . Let vector $\mathbf{c}_{i\ell} \in \mathbb{R}^M$ represent the values of M demographic factors of beat i in year ℓ . The graph \mathcal{G} is given by associating a node with every beat and connecting two nodes by an edge whenever the corresponding beats are geographically adjacent. The set of adjacency pairs is defined by $\mathcal{A} = \{(i, j) \in \mathcal{I} : i, j \text{ are adjacent in } \mathcal{G}\}$. Then, we use the spatially lagged endogenous regressors (Rosen 1974) defined as

$$\lambda_{i\ell} = \underbrace{\sum_{(i,j) \in \mathcal{A}} \alpha_{ij} \lambda_{j\ell}}_{(\dagger)} + \underbrace{\beta_0 \lambda_{i,\ell-1}}_{(\ddagger)} + \underbrace{\sum_{t=0}^p \mathbf{c}_{i,\ell-t} \boldsymbol{\beta}_t}_{(\dagger\dagger)} + \epsilon_i, \quad \ell = p+1, \dots, L, \quad (5)$$

where (\dagger) represents the influence of neighboring beats $j : (i, j) \in \mathcal{A}$, (\ddagger) represents the influence of the arrival rate in the last year, and $(\dagger\dagger)$ represents the influence of demographic factors in the past p years. The p is the total number of past years of data that we consider for fitting the regressor (in our case, $p = 1$). The spatial coefficient matrix $A = (\alpha_{ij}) \in \mathbb{R}^{I \times I}$ specifies the spatial correlation between arrival rates of two beats. The temporal coefficient $\beta_0 \in \mathbb{R}$ specifies the influence of the

arrival rate in the last year. The coefficient $\beta_t \in \mathbb{R}^M, \forall 1 \leq t \leq p$ specifies the correlation of demographic factors. Let X_i denote a subset of the data $\{\{c_{il}\}_{l \in \mathcal{L}}, \{\lambda_{jl}\}_{(i,j) \in \mathcal{A}, l \in \mathcal{L}}\}$. The error $\epsilon_i \in \mathbb{R}, i \in \mathcal{I}$ is a random noise, $\mathbb{E}[\epsilon_i | X_i] = 0$ and $\text{Cov}[\epsilon_i, \epsilon_j | X_i, X_j] = \Sigma_\theta(i, j)$ for all $i, j \in \mathcal{I}$. The spatial covariance of the noise between two beats i, j is determined by a correlation function Σ_θ , which is a function of their spatial distance s_{ij} , and is parameterized by θ . Some commonly used spatial models, including: Gaussian model (Lee et al. 2014), Exponential model (Gaetan and Guyon 2010), and Matérn model (Gaetan and Guyon 2010). Here we adopt the exponential model where $\Sigma_\theta(i, j) = \theta_1 \exp\{-\theta s_{ij}\}$, where θ is a pre-specified parameter. The other parameters of the model including $\{A, \beta_0, \{\beta_t\}_{1 \leq t \leq p}\}$ can be fitted by maximum likelihood estimation using historical data $\{X_i\}_{i \in \mathcal{I}}$.

4.2.2 On-scene Time Estimation

As we assume the on-scene time of a response unit is independent of its service region, we investigate the distribution of the on-scene time of each unit in the same zone. By looking into the data, we have seen that the on-scene time of response units follows an exponential distribution shown in Figure 7. We obtain the mean on-scene time $1/\mu = 31.2$ (minutes) by averaging the on-scene time of all dispatches in the past.

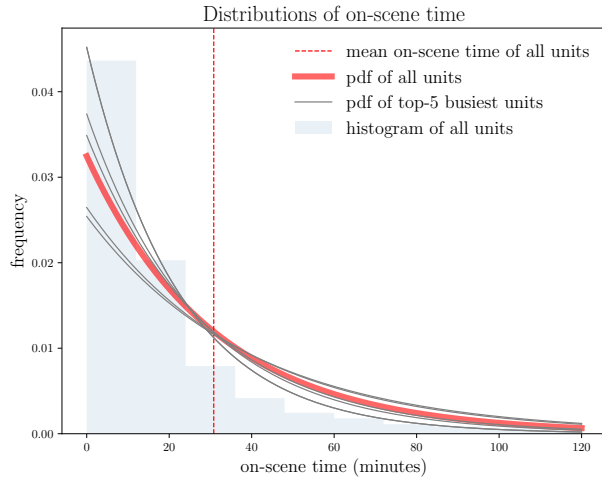


Figure 7: Distribution of the on-scene time of all units: The on-scene time data follows an exponential distribution, and it is shown by the red and grey lines. The red dash line indicates the mean on-scene time for all response units.

4.2.3 Travel Time Estimation.

We estimated the beat-to-beat travel time $T = (\tau_{ij})$ from the 911 call dispatch data. The estimation result is shown in Figure 8 by averaging the travel time of all 911 call dispatches that started in beat i and ended in beat j . In this figure, beats are ordered according to their relative location in the city. Thus, the beats in the same zone are consecutively numbered. Clearly, the figure reveals that local traveling within a neighborhood region usually taking a longer time than traveling across zones. There are two major reasons accounting for this phenomenon: first, cross-zone calls usually have higher priority, which takes less time to response, and requires more police units to assist the call (that is why sometimes they need polices from other zones); second, response units usually

resort to the highway system of the city when responding to the non-local calls, which may help reduce the travel time.

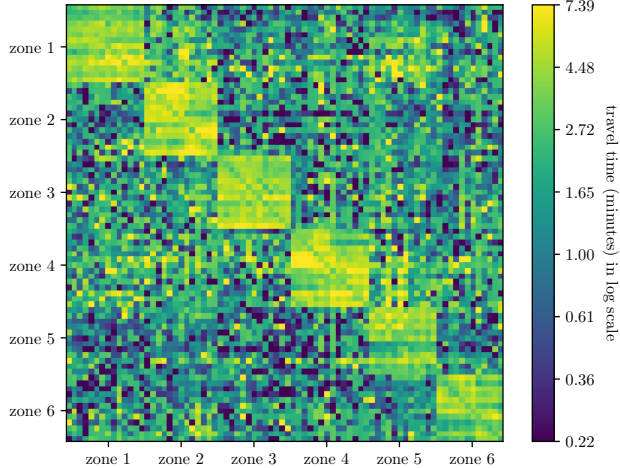


Figure 8: The *beat-to-beat* matrix $T = (\tau_{ij})$ (seconds) estimated from the real data. Each row and each column corresponds to a beat, and each small square represents average beat-to-beat travel time.

4.3 Model Validation

To evaluate the predictive accuracy of the estimated police zone workload, we compare the real zone workload reported by historical data with the out-of-sample zone workload simulation from our operations model using leave-one-out cross-validation. Specifically, the operations model defined in Section 3 takes the 911 calls arrival rates, the police service rate, and beat-to-beat travel time in a particular year as input variables and generate the simulated police workload for each zone using the existing zone design according to (4). In practice, we estimate these input quantities using the data (Section 4.1) from the past five years. The exact estimation procedures for input variables have been elaborated in Sections 4.2.1–4.2.3. Figure 9 shows comparisons for the average workload between zones and averaged workload between years. To carry out the evaluation for each zone/year in Figure 9, the model estimation is performed using all data except for one zone/year, and a prediction is made for that zone/year. The result shows that the simulation is consistent with the real data, and the percentage difference is less than 6.7%.

The simulation model allows us to quantify the impact of an arbitrary zone design on the zone workload analytically. However, it cannot be used to search for an improved zone design efficiently due to the randomness and the non-linear structures of zone workloads with respect to decisions. In Section 5.1, we will develop a way to approximate the zone workload, which can be used in the optimization.

5 Zone Design Optimization

In this section, we develop an optimization model for zone redesign. We assume that all the beat areas are given, so the zone districting decision is equivalent to a graph partition where we allocate the beats to a fixed number of zones. Recall that the matrix $D = (d_{ik})_{I \times K}$ represents the beat

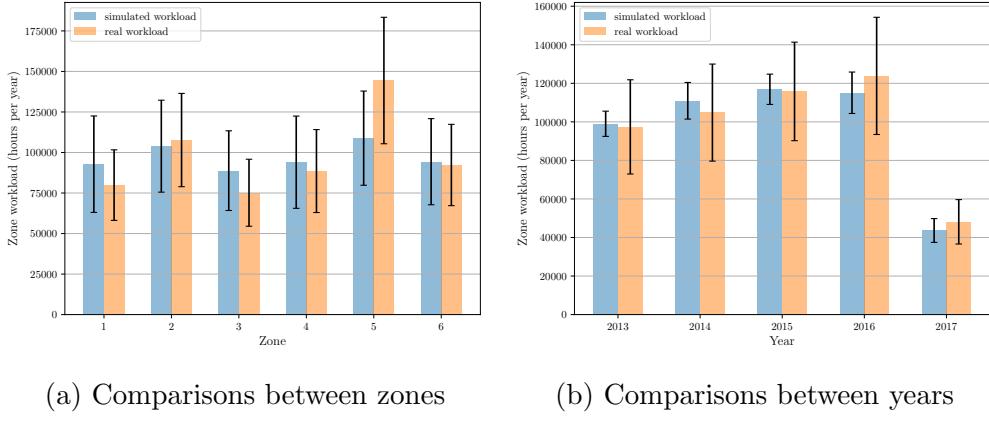


Figure 9: Validations for the operational model of annual zone workload (only first quarter data are available in year 2017) (9a). shows the averaged simulated workload for each zone ($\sum_{\ell \in \mathcal{L}} w_{k\ell}(D_0)/L$) and (9b) shows the averaged simulated workload for each year ($\sum_{k \in \mathcal{K}} w_{k\ell}(D_0)/K$).

allocation decisions, and $w^{(k)}(D)$ represents the mean police workload in zone $k \in \mathcal{K}$ given a districting design D .

Based on the discussion with the police, we choose the objective function as the workload variance among different zones, which quantitatively measure the police workload imbalance between zones from a macro view. In our study, we consider balancing police workload as one of the design objectives. Various definitions for police workload have been adopted in the literature. [Mitchell \(1972\)](#) defines police workload as the sum of service time and travel time. [Curtin et al. \(2005\)](#) uses the number or frequency of 911 calls occurring at each district as a proxy for the workload. In [Bodily \(1978\)](#) and [D'Amico et al. \(2002\)](#), the workload is defined as the fraction of working time that an agent spends attending to calls. An equivalent measure is considered by [Benveniste \(1985\)](#). Response time is also an important performance measure representing the time between the arrival of a call for service and the arrival of a unit at the incident location. According to [Bodily \(1978\)](#), the reduction of the response time results in a number of beneficial effects such as (a) increased likelihood of intercepting a crime in progress; (b) deterrent effect on criminals; and (c) increased confidence of citizens in the police. After rounds of discussion with the police officers from the Atlanta Police Department, we learned that what concerns the police department most is the workload imbalance for a medium-sized or large city like Atlanta, which usually results in police overworking in a certain region, such as Buckhead, Atlanta. In particular, longer shifts and officer fatigue may lead to a host of public safety issues and creates extra financial pressures (in the form of bonuses and overtime). Therefore, in this paper, we follow the workload definition introduced by [Mitchell \(1972\)](#), and aim to minimize the workload imbalance across zones. We also compare the waiting, travel, and response time before and after the proposed new plan was implemented as performance evaluation.

The goal is to minimize the workload variance subject to some shape constraints (e.g., contiguity

and compactness) for each zone. The zone redesign problem can be expressed as

$$\begin{aligned}
& \underset{D \in \{0,1\}^{I \times K}}{\text{minimize}} \quad f(D) := \sum_{k=1}^K \left(w^{(k)}(D) - \frac{1}{K} \sum_{k'=1}^K w^{(k')}(D) \right)^2 \\
& \text{subject to} \quad \sum_{k=1}^K d_{ik} = 1, \quad \forall i \in \mathcal{I}, \\
& \quad \text{contiguity and compactness constraints for zone } k \in \mathcal{K}.
\end{aligned} \tag{6}$$

Notice that the zone-level workload variance is chosen as the objective function in problem (6), as APD suggested this metric for their zone redesign. This metric was also used internally by APD to measure previous zone redistricting plans (Egbert 2016). However, one may also consider other performance metrics, such as mean response time or workload variance at the beat level (we provided expressions for these metrics in Section 3.3). Our framework can be similarly adapted to solve these problems.

The remainder of this section is organized as follows. First, we present a linear approximation of the workload function in Section 5.1. Then, we reformulate the objective function in a linear form in Section 5.2. Finally, we define the zone shape constraints, and formulate the problem as a mixed-integer linear program (MILP) in Section 5.3.

5.1 Zone Workload Approximation

An important challenge for solving the optimization problem (6) is characterizing the complex dependence between the decision variables $D = (d_{ik})$ and the mean zone workload $w^{(k)}(D)$. The exact relationship is specified by the hypercube queue model presented in Section 3, so in theory, one can compute the mean workload in each zone for any zone design variable D using the method in Section 3.4. However, it is impractical to carry out such computation for the purpose of zone redistricting since the decision space is extremely large. For example, with the six zones and 81 beats in Atlanta, this will generate more than 2.4×10^{59} possible zone designs.

To tackle this challenge, we consider a local approximation of the workload function, which allows the objective function of the optimization problem (6) to be expressed explicitly. Consider a given zone with an existing design. If we make a small change to this zone, e.g., by adding a few beats or removing a few beats, the workload of this zone can be approximated by its first-order Taylor expansion as

$$w^{(k)}(D) = \theta_{0k} + \sum_{i \in \mathcal{I}} \theta_{ik} d_{ik} + \tilde{\epsilon}^{(k)}, \quad \forall k \in \mathcal{K} \tag{7}$$

where $\boldsymbol{\theta} = \{\{\theta_{0k} \in \mathbb{R}\}_{k \in \mathcal{K}}, \{\theta_{ik} \in \mathbb{R}\}_{i \in \mathcal{I}, k \in \mathcal{K}}\}$ denotes the coefficients of this approximation model, and $\tilde{\epsilon}^{(k)}, \forall k \in \mathcal{K}$ represent the approximation errors.

We estimate the parameters in Eq (7) as follows. First, for each of the six zones in Atlanta, we sample 1,000 designs that are created using small perturbations from the existing design. In particular, these samples are generated by randomly changing a few beats on the boundary of the existing zone design, see Figure 10. In practice, we only consider decisions with less than six beats shift. The police would not simply accept a new plan that is a drastic departure from the existing plan for two major reasons: (1) a large-scale operational change will result in high implementation cost; (2) a radical plan will usually face significant uncertainties and unpredictable risks in the future operation. Obtaining a single sample involves procedures as follows: (a) generate a random design by changing a limited number of beat assignments; (b) compute the steady-state

probabilities of six zones by solving (1); (c) obtain simulated zone workload by computing (4). The computational bottleneck of getting one sample lies on step (b), which might take 2 minutes or so, depending on the number of the beat shifts and the computer-processing power. The entire generating process takes around 33 hours. Next, we estimate the parameters of the linear function in Eq (7) using generated data samples. More specifically, we apply the least squares method to obtain the estimated values $\hat{\theta}$, where the residual is $R^2 = 0.987$. Finally, we replace the exact workload function $w^{(k)}(D)$ with its approximation $\hat{w}^{(k)}(D|\hat{\theta}) = \hat{\theta}_{0k} + \sum_{i \in \mathcal{I}} \hat{\theta}_{ik} d_{ik}$. The objective function $f(D)$ of the optimization problem (6) is thus approximated by

$$\tilde{f}(D|\hat{\theta}) = \sum_{k=1}^K \left(\hat{w}^{(k)}(D|\hat{\theta}) - \frac{1}{K} \sum_{k'=1}^K \hat{w}^{(k')}(D|\hat{\theta}) \right)^2. \quad (8)$$

In Figure 11, we evaluate the effectiveness of our approximation by plotting the values of the objective function (i.e., workload variance) and corresponding approximations for 122 randomly selected *out-of-sample* designs. These designs are also created based on the exiting design in Atlanta: 23 of them have one beat shift, 24 of them have two beats shift, 26 of them have three and four beats shift, and the other have five-beat shifts. Note that these designs are uniformly sampled from all possibilities and not necessarily optimal for the objective. The blue dash line plots the exact objective value $\{f(D_i)\}$, calculated by simulation. The red curve plots the approximated workload value $\{\tilde{f}(D_i|\hat{\theta})\}$. The result shows that the approximated objective values match well with the true objective values for these randomly generated designs.

5.2 Linearizing Objective Function

With the parametric approximation (8), the objective function measuring the workload variance becomes a *quadratic* function of the binary decision variables D . Using a standard technique for quadratic binary variables, this quadratic function can be expressed as a linear form by introducing auxiliary variables $e_{ijkk'}$ with additional constraints

$$e_{ijkk'} \leq d_{ik}, \quad e_{ijkk'} \leq d_{jk'}, \quad e_{ijkk'} \geq d_{ik} + d_{jk'} - 1, \quad e_{ijkk'} \geq 0 \quad \text{for all } i, j \in \mathcal{I}, k, k' \in \mathcal{K}.$$

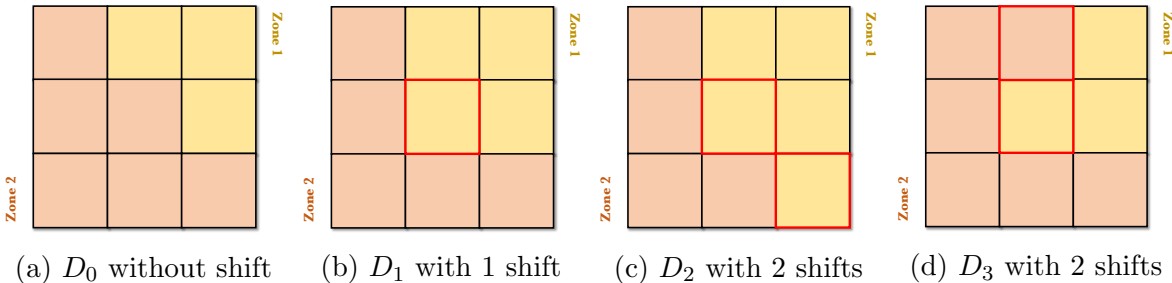


Figure 10: Examples show three local decisions by making 1, 2, 2 shifts, respectively. Each square block represents a single beat. Blocks with the same color are in the same zone. The red boxes indicate the shifts based on the original decision. (10a) shows the original decision D_0 without any shift; (10b) shows the decision D_1 with only 1 shift on the boundary; (10c, 10d) show two decisions D_2, D_3 with different 2 shifts on the boundary.

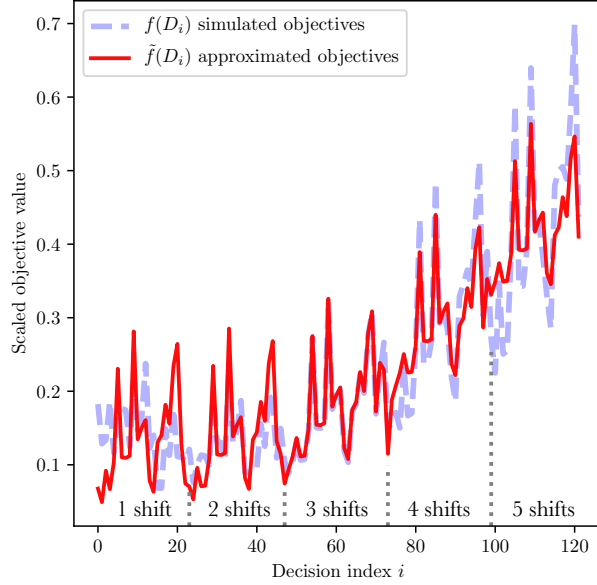


Figure 11: The approximated and simulated objective values versus a subset of $\{D_i\}$ that differs to each other by shuffling a small number of beats. Decisions indexed by $0 \leq i < 23$, $23 \leq i < 47$, $47 \leq i < 73$, $73 \leq i < 99$, $99 \leq i < 122$ correspond to randomly generated designs with 1, 2, 3, 4, and 5 shifts, respectively, comparing to the existing zone plan regarding the beat assignment.

These constraints ensure that $e_{ijkk'} = d_{ik}d_{jk'}$. Therefore, the objective function can be written as

$$\begin{aligned} \tilde{f}(D|\hat{\theta}) = & \sum_{k=1}^K \left[c^{(k)} + \sum_{i=1}^I \sum_{j=1}^I \hat{\theta}_{ik} \hat{\theta}_{jk} e_{ijkk} + 2\hat{\theta}_{0k} \sum_{i=1}^I \hat{\theta}_{ik} d_{ik} - \right. \\ & \frac{2}{K} \left(\sum_{k'=1}^K \hat{\theta}_{0k'} \right) \sum_{i=1}^I \hat{\theta}_{ik} d_{ik} - \frac{2}{K} \hat{\theta}_{0k} \sum_{k'=1}^K \sum_{i=1}^I \hat{\theta}_{ik'} d_{ik'} - \frac{2}{K} \sum_{i=1}^I \sum_{j=1}^I \sum_{k'=1}^K \hat{\theta}_{ik} \hat{\theta}_{jk'} e_{ijkk'} + \quad (9) \\ & \left. \frac{2}{K^2} \left(\sum_{k'=1}^K \hat{\theta}_{0k'} \right) \sum_{k'=1}^K \sum_{i=1}^I \hat{\theta}_{ik'} d_{ik'} + \sum_{k'=1}^K \sum_{k''=1}^K \sum_{i=1}^I \sum_{j=1}^I \hat{\theta}_{ik'} \hat{\theta}_{jk''} e_{ijk'k''} \right], \end{aligned}$$

where $c^{(k)} = \hat{\theta}_{0k}^2 + 2\hat{\theta}_{0k} \sum_{k'=1}^K \hat{\theta}_{0k'}/K + (\sum_{k'=1}^K \hat{\theta}_{0k'})^2/K^2$ is a constant term for all $k \in \mathcal{K}$. The reformulated problem itself contains more than 240,000 variables and is characterized by a large search space with more than 2.4×10^{59} possible solutions. To tackle the computational complexity of solving this large-scale MILP, consider the implementation feasibility, and avoid drastic changes from the existing zone design, we use a fast local search method based on simulated annealing. The optimization process takes about 30 to 50 minutes depending on where the problem converged given a single laptop's computational power with quad-core processors, which speed up to 4.7 GHz.

5.3 Contiguity and Compactness Constraints

In addition to balancing the police workload, it is desirable that the zone shapes are contiguous and compact. In fact, the police never used a quantitative measure of compactness to declare the

plans unsuitable. Instead, the police have disallowed plans with long and thin or snakelike districts. In other words, it appears that the police have evaluated compactness only visually. Since it is not obvious how to determine an acceptable compact design, we choose to minimize the workload variance based on the discussion with the police; but it should be understood that compactness is, in reality, a loose constraint rather than an objective. Therefore, we formulate the *contiguity* and *compactness* criteria using the following set of linear constraints, which requires beats in the same redesigned zone are geographically connected and close to each other. Moreover, two specific requirements for the design suggested by the police are also considered as constraints in our model, which are (1) beat 305, 111 should be staying in zone 3 and 1, respectively; (2) zone 3 will not take any beat from zone 4.

5.3.1 Contiguity Constraints.

We formulate the contiguity constraints using a network flow approach (see [Shirabe 2009](#)). We define a flow network, where each beat is represented by a node. An arc from node i to node j exists if the beats associated with these two nodes are geographically adjacent. Let \mathcal{A} represent the set of arcs.

We now define flow constraints for each zone $k \in \mathcal{K}$ to ensure contiguity. Let n_{\max} be the maximum number of beats allowed in a zone. If beat i belongs to zone k , i.e., $d_{ik} = 1$, we send one unit of flow into node i . Let v_{ijk} be the amount of flow from beat i to beat j if $(i, j) \in \mathcal{A}$ and both beats belong to zone k . In addition, for each zone k , we specify a special “sink node.” Let h_{ik} be 1 if beat $i \in \mathcal{I}$ is selected as the sink node in zone $k \in \mathcal{K}$; otherwise, let h_{ik} be 0. The sink node receives one unit of flow from every other node in the same zone. This ensures that there is a path of positive flow from any node in the zone to the sink node, implying contiguity. In sum, we formulate the contiguity constraints as

$$\sum_{j:(i,j) \in \mathcal{A}} v_{ijk} - \sum_{l:(l,i) \in \mathcal{A}} v_{lik} \geq d_{ik} - n_{\max}h_{ik}, \quad \forall i \in \mathcal{I}, k \in \mathcal{K}, \quad (10a)$$

$$v_{ijk} + v_{jik} \leq (n_{\max} - 1)d_{ik}, \quad \forall (i, j) \in \mathcal{A}, k \in \mathcal{K}, \quad (10b)$$

$$\sum_{i=1}^N h_{ik} = 1, \quad \forall k \in \mathcal{K}, \quad (10c)$$

$$h_{ik} - d_{ik} \leq 0, \quad \forall i \in \mathcal{I}, k \in \mathcal{K} \quad (10d)$$

$$d_{ik}, h_{ik} \in \{0, 1\}, \quad \forall i \in \mathcal{I}, k \in \mathcal{K}, \quad (10e)$$

$$v_{ijk} \geq 0, \quad \forall (i, j) \in \mathcal{A}, k \in \mathcal{K}. \quad (10f)$$

Specifically, constraints (10a) represent the net outflow from all nodes. The two terms on the left indicate, respectively, the total outflow and total inflow of beat i . If beat i is included in zone k and it is not a sink, then we have $d_{ik} = 1$, $h_{ik} = 0$, and thus beat i must have an outflow of one unit. If beat i is included in zone k and is a sink, then we have $d_{ik} = 1$, $h_{ik} = 1$, and thus beat i has a negative outflow lower bounded by $1 - n_{\max}$. Constraints (10b) ensure that if beat i is not in zone k , i.e. $d_{ik} = 0$, there must be no flow into or out of beat i with any nodes in zone k ; if beat i is in zone k (i.e. $d_{ik} = 1$), the flow between two beats does not exceed $n_{\max} - 1$. Constraints (10c) ensure that each zone must have a unique sink node. Constraints (10d) ensure that beat i must belong to zone k if it is the sink for that zone. These constraints together ensure that each zone is contiguous.

5.3.2 Compactness Constraints

We consider two ways to enforce the compactness of each zone: distance compactness (Niemi 1990, Yong 1988) and shape compactness (Garfinkel and Nemhauser 1970). For distance compactness, we require the distance between any two beats in a zone to be bounded by some parameters. For shape compactness, we require the square of the diameter divided by the zone's area to be upper bounded by another parameter. These constraints can be formulated as follows.

For each beat $i \in \mathcal{I}$, let A_i be its area. For each pair of beats $(i, j) \in \mathcal{I} \times \mathcal{I}$, let l_{ij} be the square of the distance between the center of these beats. We choose two parameters $\zeta_1, \zeta_2 > 0$ to control the level of distance compactness and shape constraints, respectively. Then we have

$$l_{ij}e_{ijkk} \leq \zeta_1, \quad \forall i \in \mathcal{I}, j \in \mathcal{I}, k \in \mathcal{K}, \quad (11a)$$

$$l_{ij}e_{ijkk} \leq \zeta_2 \sum_{i=1}^K d_{ik}A_i, \quad \forall i \in \mathcal{I}, j \in \mathcal{I}, k \in \mathcal{K}. \quad (11b)$$

Recall that $e_{ijkk} = d_{ik}d_{jk}$ is equal to 1 if both beat i and beat j are in zone k , and is equal to 0 otherwise. Constraints 11a represent the distance compactness criterion. Constraints 11b represent the shape compactness criterion, where $\sum_{i=1}^K d_{ik}A_i$ is the area of zone $k \in \mathcal{K}$.

Altogether, combining the contiguity constraints (10) and the compactness constraints (11), and substituting (9) into the objective function of problem (6), we obtain the complete mixed-integer linear programming (MILP) formulation of the zone districting design problem. To ease the implementation of zone redistricting, APD specified that our proposed new plan should not make major changes to the existing zone configuration. Therefore, after we obtain the solution to the mixed-integer linear program, we use a local search to tune the output of the model so that our solution is close to the existing configuration and satisfy the requirement of APD.

6 Implementation Results

6.1 Workload Imbalance Analysis

As we mentioned in Section 1, under the previous zone design in Atlanta, the workload imbalance across zones had worsened in the past few years. This imbalance issue is partly due to the growth and movement of population, as well as changing (mostly worsening) traffic conditions. Here, we analyze how zone configuration affects the workload imbalance over the years, and predict the future trend if there is no change in the configuration. To quantify the imbalance of workload, we use the variance of workload across zones as the metric, which is defined in Section 5. Recall that this metric is equal to the sum of the squared deviation of annual zone workload from city-wide mean workload, i.e., $\sum_{k=1}^K (w^{(k)} - (\sum_{k'=1}^K w^{(k')})/K)^2$.

We computed the actual workload from the year 2014 to 2017 (the most recent year at the time of our redesign process) from the police report data, as well as the predicted workload for the year 2018 and 2019 using the method described in Sections 3 and 4. The workload in each beat is displayed on the city map in Figure 12. There is a clear trend that the workload was growing city-wide over the years. Moreover, the workload was particularly high in several concentrated areas, such as Buckhead in Zone 2, Midtown in Zone 5, and the intersection of highway I-285 and highway I-20 in zone 4.

In Figure 13, we plot the total workload of the entire city (red curve) and the workload imbalance across the six zones (blue curve). As before, the data for 2018 and 2019 are based on predictions.

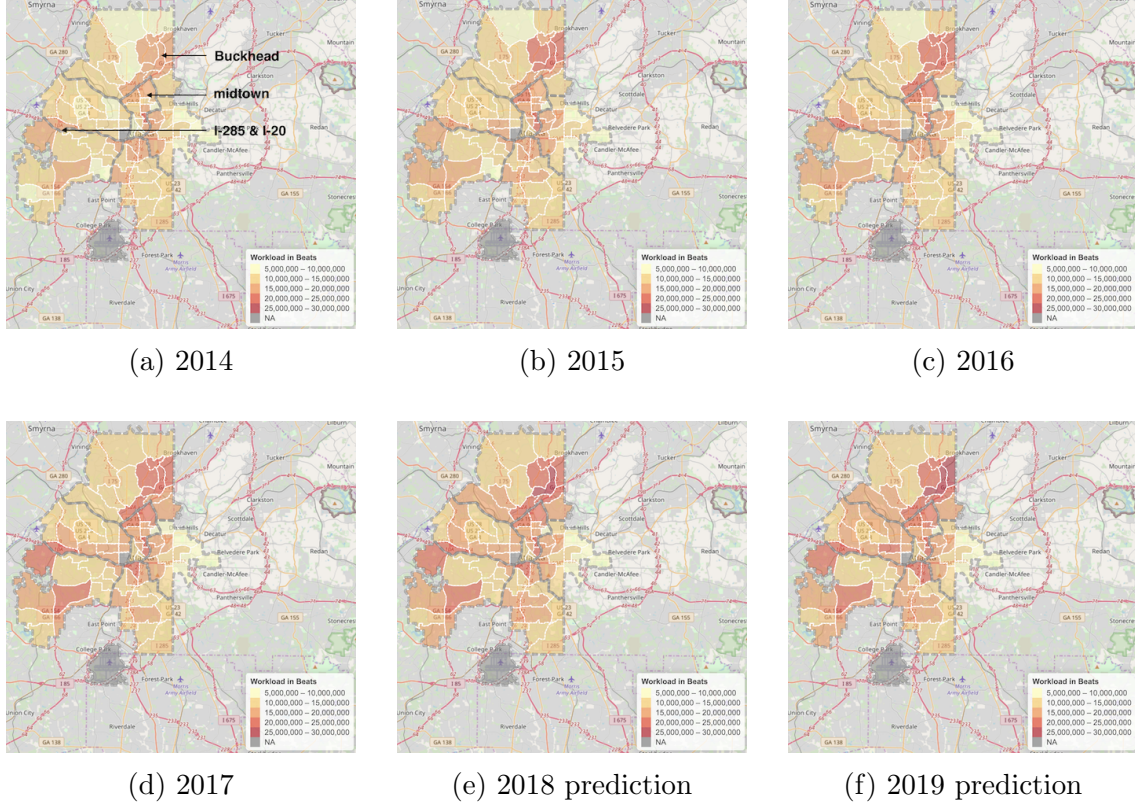


Figure 12: The beat level workload (in seconds) in Atlanta from the year 2014 to 2019. Dashed grey lines represent the boundaries of the six zones. Darker color means a higher workload. (The gray area at the bottom corresponds to the Atlanta International Airport, which we exclude from our analysis.)

The result shows that both the total workload and the workload variance would have increased without zone reconfiguration.

6.2 Zone Reconfiguration

Using the approach outlined in Sections 3–5, we propose a new police zone plan for Atlanta. The initial report in 2018 contained beat-wise workload prediction for the next two years (2018 and 2019) and proposed three candidate designs with similar beat shifts that all attain the best workload balance. In Table 2, we list the predicted annual workload in each zone, total workload, and workload variance. After the plan was reported to the police, we met several times to deliberate the various trade-offs and held police-engagement meetings to elicit feedback from the patrol force. Police Deputy Chief and couples of key senior officers also participated in these discussions and voiced comments. After several rounds of discussions, the police chose one of our proposed designs as the new police zone configuration. The new design and the previous design are shown side-by-side in Figure 14. The police prefer this design for three major reasons: (1) this plan makes minimal changes (only four beats assignments being shifted) based on the existing police zone configuration in comparison with other candidate plans, which minimizes the implementation cost in practice; (2) beat 203 and 213 are two areas with relatively low police workload in zone 2. Moving them out of zone 2 may help focus their police resources on curbing the crime surge in the Buckhead area

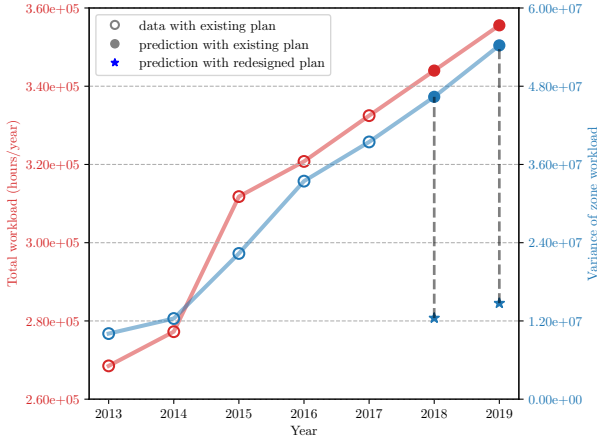


Figure 13: The total workload of all zones (red) and variance of workload across zones (blue) from the year 2013 to 2019: The dots for 2018 and 2019 are predicted levels assuming the configuration is not changed, and the stars for the year 2018 and 2019 are predicted levels under our proposed redesigned configuration.

Table 2: Comparison of the predicted workload under the previous zone design and the new zone design.

	Workload ($\times 10^4$ hrs/yr)						Variance ($\times 10^7$)	Variance increase ratio compare with 2016 (%)
	Zone 1	Zone 2	Zone 3	Zone 4	Zone 5	Zone 6	Total	
Real 2016	5.3744	6.0082	5.3891	5.6164	5.5479	4.1413	32.0776	3.3441
Real 2017	5.6648	6.2981	5.5154	5.7919	5.7319	4.2454	33.2479	3.9454
Predicted 2018	5.9558	6.5833	5.6366	5.9606	5.9143	4.3488	34.3996	4.6375
Predicted 2019	6.2487	6.8650	5.7642	6.1292	6.0976	4.4518	35.5568	5.4267
Predicted 2018 with redesign	5.9018	5.6961	5.6366	5.9606	6.1595	5.0448	34.3996	1.2442
Predicted 2019 with redesign	6.1833	5.9294	5.7642	6.1292	6.3686	5.1819	35.5568	1.4721

(the center of zone 2); (3) zone 3 and 4 have maintained a good operational balance for the recent years. Keeping these two zones intact can also help reduce the implementation cost of the plan. For both predictions in 2018 and 2019, the redesigned zone plan has a more balanced workload distribution over the six zones, as the colors are more uniform. The new design is projected to reduce the workload variance drastically by 83% and 86% for the year 2018 and 2019, respectively.

6.3 Implementation and Impact

In January 2019, we submitted the final report for zone redesign to the Atlanta Police Department, which was reviewed by the Police Chief and her team. Our report analyzed the annual growth trend of police workload and proposed a detailed redistricting plan. Our redistricting plan involves changing four zones: Zone 6 in East Atlanta will increase by four square miles. Zone 1 in Northwest Atlanta will increase by two square miles. Zone 2, which covers Northeast Atlanta and Buckhead, decreases by seven square miles. Zone 5 also has some minor changes. The detailed plan is shown in Figure 14. Overall, the redistricting rebalanced the police workload between the four zones and reduced the average response time in Zone 2 (Habersham 2019).

In February 2019, Atlanta's City Council voted to approve our proposed redistricting plan. The Atlanta Police Department officially implemented the plan on March 17, 2019. In a statement about

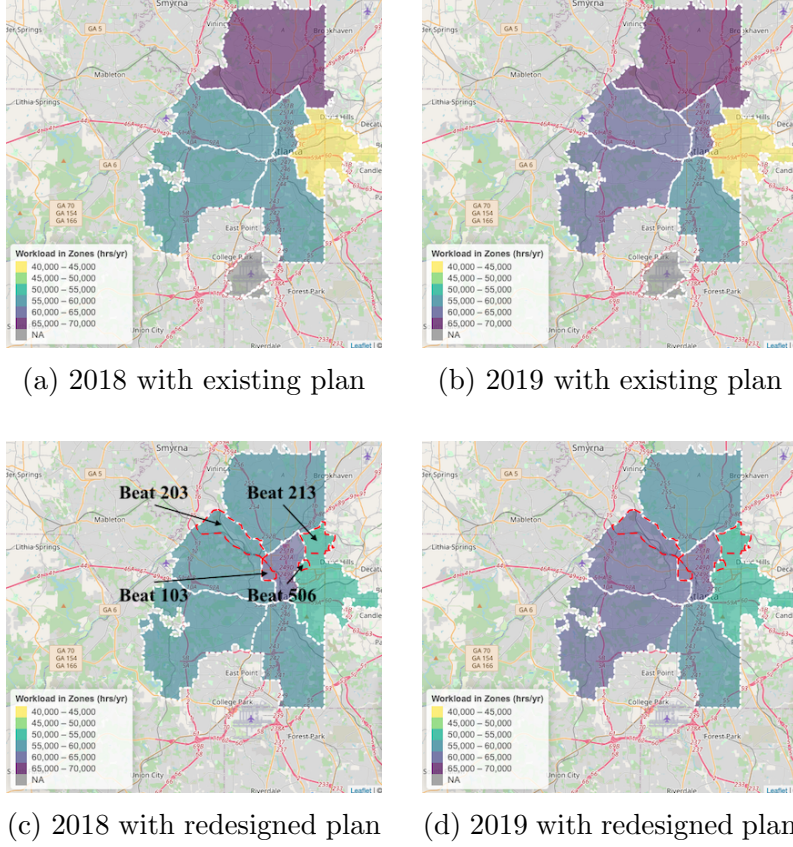
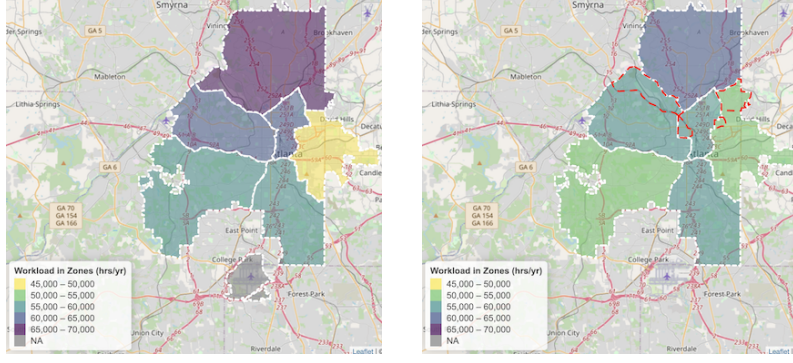


Figure 14: Comparison of zone workload distribution between the existing plan and the redesigned plan: for 2018 and 2019 (based on prediction), respectively. The color depth of each zone represents the level of its annual workload. Beat shifts in the redesigned plans have been highlighted by red dash lines. As we can see, for the predicted year 2018 and 2019, the redesigned plan achieves a more balanced workload across zones comparing to the existing plan.

Table 3: Comparison of the real workload before and after the redesign.

Time period	Workload ($\times 10^4$ hrs/yr)							Variance ($\times 10^7$)	Variance increase year-on-year ratio (%)
	Zone 1	Zone 2	Zone 3	Zone 4	Zone 5	Zone 6	Total		
Mar 2018 ~ Mar 2019 (before)	6.0568	6.8737	5.5450	5.7040	6.1607	4.7360	35.0762	4.2375	+7.40
Mar 2019 ~ Mar 2020 (after)	5.5142	6.3753	5.7157	5.0090	5.9462	5.0129	33.5733	2.3925	-43.54

this redesign (Atlanta Police Department 2019), the APD Deputy Chief Jeff Glazier stated that: “It is important that we examine our officer workload periodically, and with the help of Georgia Tech we were able to do so in a data-driven manner. We are confident these changes will balance the workload in all zones.” The new zone design was the amount of time spent on processing the incidents also covered by several media outlets, including the Atlanta Journal Constitution (AJC), the largest daily newspaper in the Atlanta metropolitan area. Residents of Atlanta praised the change on social media and thanked Atlanta Police and our team for contributing to the communities (Rosete 2019).



(a) before redesign

(b) after redesign

Figure 15: Zone workload distribution before and after the redesign according to the post-implementation data ranging from 2017 March to 2020 March by APD. Beat shifts in the redesigned plans have been highlighted by red dash lines. For beats moving out of zone 2 (beat 204 and 213), their workloads have been increased by 45.61% and 48.95%, respectively; For beat 506 moved from zone 5 to zone 6, its workload has been increased by 19.00%; And for beat 103 moved from zone 1 to zone 5, its workload has been reduced by 4.71%.

6.4 Post-implementation Analysis

In August 2020, we received the most recent 911 call data released by the Atlanta Police Department thanks to Major John Quigley’s help. This new data set has the same format as we described in Section 4.1 and contains consistent records from the pre-implementation period since we finalized this study (March 2017 ~ March 2019) to the post-implementation period (March 2019 ~ March 2020). We exclude the data after March 2020 due to the fact that police operations are drastically affected by the COVID-19 pandemic and the citywide lockdown. Also, due to the inconsistency between the new data set and the previous records, we normalize the new data set to bring the workload of each zone in the overlapping period (the year 2017) to the same range recorded by the previous records. The data provides insights into what has changed in response to the districting and offers a unique opportunity to study the ultimate social impact resulted from the police zone redesign. By taking advantage of this data set, we first re-evaluate the zone workload distribution and the workload variance $f(D)$ defined in (6) before and after the implementation and check whether the workload imbalance between zones has been improved or not. Apart from the workload analysis, we also focus on three other metrics as we described in Section 3.1, i.e., waiting time, travel time, and response time (the sum of waiting time and travel time). We do not study on-scene time since it is normally unrelated to the districting. In particular, response time plays a big role in public satisfaction and directly reflects the effectiveness of the districting plan. Complaints of poor police response time may be taking a back seat to concerns about other aspects of police conduct, but getting to that 911 call in a timely manner can be the best community relations tool of all.

In Table 3, we summarize the workload of each zone and their variances before and after the redesign officially implemented in March 2019. In Figure 15, we also visualize the workload of each zone for these three years on the map of Atlanta. As we can observe, our redesign successfully tempered growth and curbed the deterioration of workload imbalance after being officially implemented, where the workload variance of the recent year (2019) has fallen back to a normal level and reduced by 43.54% comparing to the previous year. For zone 2, particularly as the key engine of Atlanta’s economic growth, this region’s crime rate is soaring in recent years. Our new plan

Table 4: Average response, waiting, and travel time per call for all cases in six zones.

Category	Time period	Time per call (minutes)						Time increase year-on-year ratio (%)
		Zone 1	Zone 2	Zone 3	Zone 4	Zone 5	Zone 6	
Response	Mar 2018 ~ Mar 2019 (before)	30.35	32.21	27.81	30.70	30.42	26.07	29.69 +11.70
	Mar 2019 ~ Mar 2020 (after)	28.72	24.77	24.70	28.59	36.20	33.25	31.26 +5.29
Waiting	Mar 2018 ~ Mar 2019 (before)	18.41	17.75	16.61	17.87	17.97	14.21	17.24 +12.83
	Mar 2019 ~ Mar 2020 (after)	18.00	13.96	14.63	16.56	21.74	19.63	19.08 +10.67
Travel	Mar 2018 ~ Mar 2019 (before)	8.20	7.88	7.49	8.60	6.80	6.27	7.50 +28.21
	Mar 2019 ~ Mar 2020 (after)	7.56	6.02	7.28	7.51	5.98	6.27	7.43 -0.93

Table 5: Average response, waiting, and travel time per call for the highest priority calls in six zones.

Category	Time period	Time per call (minutes)						Time increase year-on-year ratio (%)
		Zone 1	Zone 2	Zone 3	Zone 4	Zone 5	Zone 6	
Response	Mar 2018 ~ Mar 2019 (before)	11.94	11.61	10.91	12.99	13.57	9.81	11.90 +10.90
	Mar 2019 ~ Mar 2020 (after)	13.92	10.59	12.06	9.36	10.34	9.80	11.21 -5.80
Waiting	Mar 2018 ~ Mar 2019 (before)	3.49	3.16	4.69	3.22	3.39	2.46	3.55 +36.02
	Mar 2019 ~ Mar 2020 (after)	4.91	2.38	3.41	3.31	2.95	3.29	3.47 -2.25
Travel	Mar 2018 ~ Mar 2019 (before)	8.48	9.55	17.73	9.45	10.05	7.08	10.72 -0.74
	Mar 2019 ~ Mar 2020 (after)	9.59	8.64	8.28	7.73	6.59	7.36	8.07 -24.72

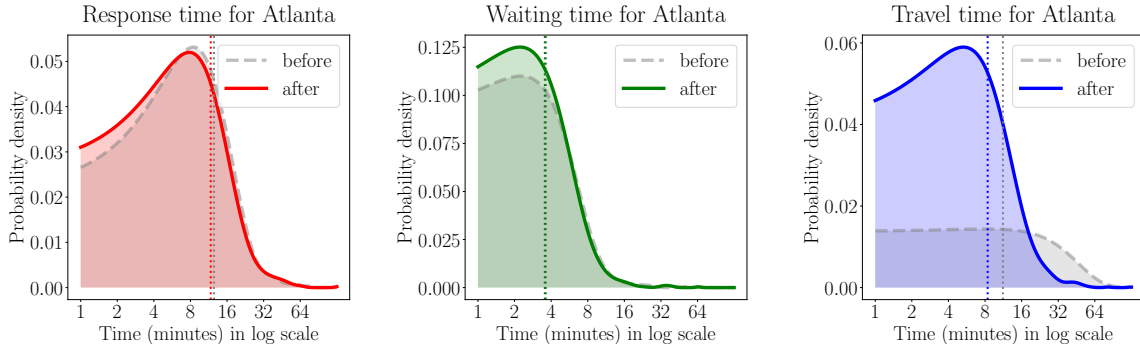


Figure 16: Distribution of response, waiting, and travel time per call for the highest priority calls before and after the redesign, calculated by kernel density estimation. Vertical dotted lines indicate the meantime of corresponding distributions. The time has been shown on a log scale to display more details within 10 minutes.

has remarkably reduced its police workload in the latest year down to a historically low level with 6.3753×10^4 hours and fell by 7.25% comparing to the last year.

In Table 5 and Table 4, we report the average response, waiting, and travel time per call for the highest priority calls and all the calls in Atlanta. In recent years, fast economic and population growth imposed additional burdens on the transportation system and police operations in Atlanta. As we can see that all three times of all calls continue increasing for the last three years in a row. However, the increasing response and waiting time rates turned lower and declined into late 2019 after our plan was officially implemented. In particular, all three times of the highest priority calls have been largely reduced compared to the previous year. For zone 2, the response time has fallen back to 10.59 minutes per call in the latest year. Figure 16, we also show the distributions of three times of the highest priority calls as we can see that the redesign has resulted in the probability

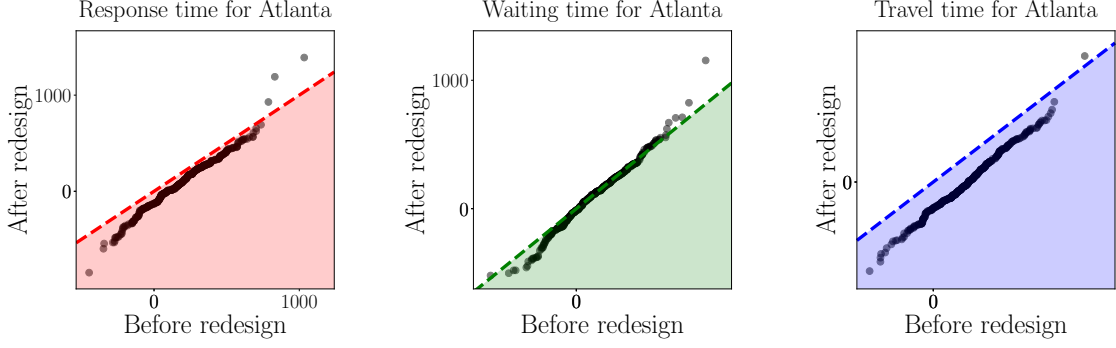


Figure 17: The difference in difference (DID) of variance for response time (red), waiting time (green), and travel time (blue) in Atlanta. For each scatter plot, the point represents one of 365 days in one year, the x -axis corresponds to the variance difference between the year 2017 and 2018 for that day, and the y -axis corresponds to the variance difference between year 2018 and 2019 for that day. The dashed line passes through the origin with a slope of 1. The point on the dashed line indicates the variance difference of that day remains consistent before and after the redesign. Point in the lower half of the (shaded) region indicates the increasing rate of variance has been reduced after the redesign.

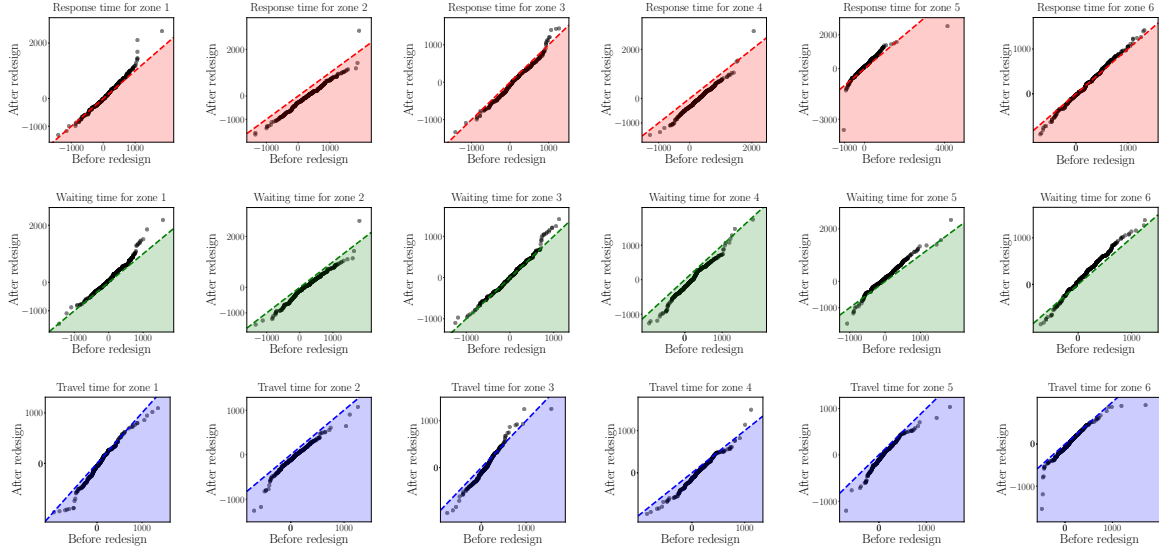


Figure 18: Difference in difference (DID) of variance for response time (1st row), waiting time (2nd row), and travel time (3rd row) in each zone.

mass of all three times being moving left toward zero.

We also perform the *difference in difference* (DID) analysis for the variance of response, waiting, and travel time and further confirm that our new plan is also helping slow the growth of imbalance of these three times over zones. To be specific, we calculate the variance of these times on each day of a year and compare the difference of variance between the pair of the year 2017 and 2018 and the pair of the year 2018 and 2019 on a daily basis. The difference of the first pair indicates the increasing rate of variance before the redesign, and the difference of the second pair indicates the

rate after the redesign. In Figure 17, we report this comparison for the entire Atlanta. For travel time, the result shows that the variance difference for most days between year 2018 and 2019 is significantly lower than the difference between year 2017 and 2018 (most of the points are below and away from the dashed line). For response and waiting time, it's also shown that these two times slowed the pace of increasing variance. In Figure 18, we have shown the same comparison from a micro-level view for each zone. For regions including zone 2, 3, and 4, where we have seen a surge in crime rate and police workload in recent two years (2017, 2018) as shown in Figure 15, the variance for all three times has significantly curbed growth. As the traditionally low-crime area, the variance increase in zone 6 has been controlled within a reasonable range. Last, for other regions, including zone 1 and 5, the variance differences have remained consistent.

7 Conclusion

In this paper, we presented a data-driven framework for police zone redistricting. The framework includes three main components: a spatially distributed queueing model for police patrol and emergency response operations, a statistical model to predict emergency call arrivals and police service rates, and a mixed-integer linear programming model for zone districting optimization. We applied this framework to redesigning police zones in Atlanta. According to our model prediction, the proposed new plan can drastically reduce workload variance by only changing four beats (about 5% of all beats). The Atlanta Police Department officially adopted our proposed redesign plan in March 2019.

Our approach can also be applied to other cities in the world that have a similar police patrol system, such as New York. We proposed a districting plan using the same method for the police department of South Fulton, another city in southwest Fulton County, Georgia, which has also been officially adopted in early 2020. We recognize that the idea of combining data analysis, stochastic model, and mixed-integer linear programming can also be used in a wide range of other types of emergency systems, including emergency medical services, fire alarm system, taxi dispatch system, et cetera.

We are also aware of four major limitations in our approaches: (1) Travel time in our model is considered to be constant over year due to lack of fine-grained traffic data; (2) We also found in the post-implementation data that the zone reconfiguration may pose a substantial impact on the occurrence of 911 calls for a certain area, which we didn't take into consideration in our model; (3) There may have been a number of exogenous factors that affect the spatio-temporal dynamics of crime rates, which are too intricate to be captured by a linear predictive model; (4) We assume the beats are fixed and formulate the problem as an integer programming to find each beat's optimal assignment. This might be limited for some cities if their police departments need a more flexible beat design.

Acknowledgement

We are grateful to Chief Erika Shields, Major John Quigley, Captain Jacquelyn Gwinn-Villaroel, and other police officers at the Atlanta Police Department for their valuable suggestions and help to make data available during the planning and development of our research. The research is partially funded by the Atlanta Police Foundation.

References

Atlanta Police Department (2019). Atlanta police make changes to four zone boundaries as part of beat redesign. <http://www.atlantapd.org/Home/Components/News/News/190/> (accessed May 1, 2020).

Atlanta Police Department (2020). Atlanta police department zones. <https://www.atlantapd.org/community/apd-zones> (accessed May 1, 2020).

Bammi, D. (1975). Allocation of police beats to patrol units to minimize response time to calls for service. *Computers & Operations Research*, 2(1):1–12.

Benveniste, R. (1985). Solving the combined zoning and location problem for several emergency units. *Journal of the Operational Research Society*, 36(5):433–450.

Bodily, S. E. (1978). Police sector design incorporating preferences of interest groups for equality and efficiency. *Management Science*, 24(12):1301–1313.

Bucarey, V., Ordóñez, F., and Bassaletti, E. (2015). Shape and balance in police districting. In *Applications of Location Analysis*, pages 329–347. Springer.

Camacho-Collados, M., Liberatore, F., and Angulo, J. M. (2015). A multi-criteria police districting problem for the efficient and effective design of patrol sector. *European journal of operational research*, 246(2):674–684.

Chaiken, J. M. and Larson, R. C. (1972). Methods for allocating urban emergency units: a survey. *Management Science*, 19(4-part-2):110–130.

Chelst, K. and Jarvis, J. P. (1979). Estimating the probability distribution of travel times for urban emergency service systems. *Operations Research*, 27(1):199–204.

Chen, H., Cheng, T., and Ye, X. (2019). Designing efficient and balanced police patrol districts on an urban street network. *International Journal of Geographical Information Science*, 33(2):269–290.

Cheung, C.-Y., Yoon, H., and Chow, A. H. (2015). Optimization of police facility deployment with a case study in greater london area. *Journal of Facilities Management*.

Chow, A. H., Cheung, C., and Yoon, H. (2015). Optimization of police facility locationing. *Transportation research record*, 2528(1):60–68.

Curtin, K. M., Hayslett-McCall, K., and Qiu, F. (2010). Determining optimal police patrol areas with maximal covering and backup covering location models. *Networks and Spatial Economics*, 10(1):125–145.

Curtin, K. M., Qui, F., Hayslett-McCall, K., and Bray, T. M. (2005). Integrating gis and maximal covering models to determine optimal police patrol areas. In *Geographic information systems and crime analysis*, pages 214–235. IGI Global.

D'Amico, S. J., Wang, S.-J., Batta, R., and Rump, C. M. (2002). A simulated annealing approach to police district design. *Computers & Operations Research*, 29(6):667–684.

Edwards, E. (2016). Predictive policing software is more accurate at predicting policing than predicting crime. <https://www.aclu.org/blog/criminal-law-reform/reforming-police/predictive-policing-software-more-accurate-predicting>.

Egbert, J. (2016). Beat redistricting proposal 2016. Atlanta Police Department (internal report).

Ferland, J. A. and Guénette, G. (1990). Decision support system for the school districting problem. *Operations Research*, 38(1):15–21.

Fritz, J. (2018). What is the average police response time in the U.S.? (accessed April 30, 2019). <https://www.safesmartliving.com/home-security/average-police-response-time/>.

Gaetan, C. and Guyon, X. (2010). *Spatial statistics and modeling*, volume 90. Springer.

Garfinkel, R. S. and Nemhauser, G. L. (1970). Optimal political districting by implicit enumeration techniques. *Management Science*, 16(8):B-495–B-508.

Gass, S. I. (1968). On the division of police districts into patrol beats. In *Proceedings of the 1968 23rd ACM National Conference*, pages 459–473. ACM.

Green, L. V. and Kolesar, P. J. (2004). Anniversary article: Improving emergency responsiveness with management science. *Management Science*, 50(8):1001–1014.

Grofman, B. (1985). Criteria for redistricting: A social science perspective. *UCLA Law Review*, 33:77–184.

Habersham, R. (2019). Atlanta police hope changes to patrol zones shorten response times. *The Atlanta Journal-Constitution*. <https://www.ajc.com/news/local/atlanta-police-change-zoning-boundaries-help-with-response-times/R4hjqmYEmaveOgkW6NfRU0/>.

Habersham, R. and Deere, S. (2019). Buckhead residents confront mayor, police chief about crime. *The Atlanta Journal-Constitution*. <https://www.ajc.com/news/local/buckhead-residents-confront-mayor-police-chief-about-crime/5VYluSvFkIAmqUloAIIRSK/>.

Hess, S. W., Weaver, J., Siegfeldt, H., Whelan, J., and Zitlau, P. (1965). Nonpartisan political redistricting by computer. *Operations Research*, 13(6):998–1006.

Jarvis, J. P. (1975). *Optimization in stochastic service systems with distinguishable servers*. PhD thesis, Massachusetts Institute of Technology.

Kistler, A. (2009). Tucson police officers redraw division boundaries to balance their workload. *Geography & Public Safety*, 1(4):3–5.

Larson, R. C. (1972). *Urban police patrol analysis*, volume 28. MIT Press Cambridge, MA.

Larson, R. C. (1974a). A hypercube queuing model for facility location and redistricting in urban emergency services. *Computers & Operations Research*, 1(1):67 – 95.

Larson, R. C. (1974b). Illustrative police sector redesign in district 4 in boston. *Urban Analysis*, 2(1):51–91.

Larson, R. C. and Odoni, A. R. (1981). *Urban Operations Research*. Prentice Hall, NJ.

Lee, M. L., Goldsman, D., Kim, S.-H., and Tsui, K.-L. (2014). Spatiotemporal biosurveillance with spatial clusters: control limit approximation and impact of spatial correlation. *IIE Transactions*, 46(8):813–827.

Levine, E., Tisch, J., Tasso, A., and Joy, M. (2017). The New York City police department’s domain awareness system. *Interfaces*, 47(1):70–84.

Liberatore, F. and Camacho-Collados, M. (2016). A comparison of local search methods for the multicriteria police districting problem on graph. *Mathematical Problems in Engineering*, 2016.

Mehrotra, A., Johnson, E. L., and Nemhauser, G. L. (1998). An optimization based heuristic for political districting. *Management Science*, 44(8):1100–1114.

Mills, G. (1967). The determination of local government electoral boundaries. *Operations Research Quarterly*, 18:243–255.

Mitchell, P. S. (1972). Optimal selection of police patrol beats. *Journal of Criminal Law, Criminology & Police Science*, 63:577.

Morrill, R. L. (1973). Ideal and reality in reapportionment. *Annals of the Association of American Geographers*, 63:463–477.

Morrill, R. L. (1976). Redistricting revisited. *Annals of the Association of American Geographers*, 66:548–556.

Nagel, S. S. (1972). Computers and the law and policies of redistricting. *Polity*, 5:77–93.

New York City Government (2020). NYPD precincts and sectors. <https://data.cityofnewyork.us/Public-Safety/NYPD-Sectors/eizi-ujye>.

Niemi, R. G., e. a. (1990). Measuring compactness and the role of a compactness standard in a test for partisan and racial gerrymandering. *The Journal of Politics*, 52(4):1155–1181.

Perry, W. L., McInnis, B., Price, C. C., Smith, S. C., and Hollywood, J. S. (2013). *Predictive policing: The role of crime forecasting in law enforcement operations*. Rand Corporation.

Piyadasun, T., Kalansuriya, B., Gangananda, M., Malshan, M., Bandara, H. D., and Marru, S. (2017). Rationalizing police patrol beats using heuristic-based clustering. In *2017 Moratuwa Engineering Research Conference (MERCon)*, pages 431–436. IEEE.

Ríos-Mercado, R. Z. (2020). *Optimal Districting and Territory Design*, volume 284. Springer.

Rosen, S. (1974). Hedonic prices and implicit markets: Product differentiation in pure competition. *Journal of Political Economy*, 82(1):34–55.

Rosete, A. (2019). People's response to the beat redesign on Nextdoor. <https://nextdoor.com/agency-post/ga/atlanta/atlanta-police-department/atlanta-police-make-changes-to-three-zone-boundaries-as-part-of-beat-redesign-104899950/>.

Sarac, A., Batta, R., Bhadury, J., and Rump, C. (1999). Reconfiguring police reporting districts in the city of buffalo. *OR Insight*, 12(3):16–24.

Saunders, J., Hunt, P., and Hollywood, J. S. (2016). Predictions put into practice: a quasi-experimental evaluation of chicago's predictive policing pilot. *Journal of Experimental Criminology*, 12(3):347–371.

Shirabe, T. (2009). Districting modeling with exact contiguity constraints. *Environment and Planning B: Planning and Design*, 36(6):1053–1066.

United States Census Bureau (2018). 2018 population estimates program. <https://factfinder.census.gov>.

Vickrey, W. (1961). On the prevention of gerrymandering. *Political Science Quarterly*, 76:105–110.

Weaver, J. B. and Hess., S. W. (1963). Districting modeling with exact contiguity constraints. *The Yale Law Journal*, 72:288–308.

Yong, H. P. (1988). Measuring the compactness of legislative districts. *Legislative Studies Quarterly*, 13:105–115.